Marine Geology 279 (2011) 19–36

Contents lists available at ScienceDirect

Marine Geology

journal homepage: www.elsevier.com/locate/margeo

Permeability–porosity relationships of subduction zone sediments

Kusali Gamage [a,*], Elizabeth Screaton [a], Barbara Bekins [b], Ivano Aiello [c]

[a] Department of Geological Sciences, University of Florida, USA
[b] U.S. Geological Survey, Menlo Park, CA, USA
[c] Moss Landing Marine Laboratories, Moss Landing CA, USA

ARTICLE INFO

Article history:
Received 30 March 2010
Received in revised form 10 October 2010
Accepted 12 October 2010
Available online 14 December 2010

Communicated by D.J.W. Piper

Keywords:
permeability
porosity
subduction zone
marine sediment
grain size
smectite

ABSTRACT

Permeability–porosity relationships for sediments from the northern Barbados, Costa Rica, Nankai, and Peru subduction zones were examined based on sediment type, grain size distribution, and general mechanical and chemical compaction history. Greater correlation was observed between permeability and porosity in siliciclastic sediments, diatom oozes, and nannofossil chalks than in nannofossil oozes. For siliciclastic sediments, grouping of sediments by percentage of clay-sized material yields relationships that are generally consistent with results from other marine settings and suggests decreasing permeability as percentage of clay-sized material increases. Correction of measured porosities for smectite content improved the correlation of permeability–porosity relationships for siliciclastic sediments and diatom oozes. The relationship between permeability and porosity for diatom oozes is very similar to the relationship in siliciclastic sediments, and permeabilities of both sediment types are related to the amount of clay-size particles. In contrast, nannofossil oozes have higher permeability values by 1.5 orders of magnitude than siliciclastic sediments of the same porosity and show poor correlation between permeability and porosity. More indurated calcareous sediments, nannofossil chalks, overlap siliciclastic permeabilities at the lower end of their measured permeability range, suggesting similar consolidation patterns at depth. Thus, the lack of correlation between permeability and porosity for nannofossil oozes is likely related to variations in mechanical and chemical compaction at shallow depths. This study provides the foundation for a much-needed global database with fundamental properties that relate to permeability in marine settings. Further progress in delineating controls on permeability requires additional carefully documented permeability measurements on well-characterized samples.

1. Introduction

Physical properties of marine sediments have been widely studied both in academic and industrial research. With the introduction of the Deep Sea Drilling Project (DSDP) and the Ocean Drilling Program (ODP), new levels of understanding have been added to the knowledge about marine sediments during the past few decades. Physical properties of submarine sediments have been studied through recovered cores, down-hole logging, and also by in-situ instrumentation and testing. Permeability is one such physical property that has been closely studied because of its importance in fluid flow and pore pressures in the subsurface. A number of investigations have focused on subduction zones because fluid flow and overpressures play an important role in thermal and solute transport and are thought to affect deformation and earthquakes (e.g. Bekins et al., 1995; Fisher and Hounslow, 1990; Hubbert and Rubey, 1959). Investigations based on numerical modeling have shown that permeability is a crucial parameter to accurately simulate fluid flow and overpressure development in subduction zone settings (e.g. Bekins et al., 1995; Bruckmann et al., 1997; Saffer and Bekins, 1998; Gamage and Screaton, 2006; Matmon and Bekins, 2006).

Sediments vary in permeability by several orders of magnitude based on factors related to composition, grain size and the overall mechanical and chemical compaction history of the sediment. For example, permeability data presented in Neuzil (1994) for argillaceous sediments indicate as much as nine orders of magnitude variation. Spinelli et al. (2004) show similar permeability variations for marine argillaceous sediments and a lesser degree of variation (five orders of magnitude) for carbonate-rich sediments. Prior to the availability of core samples of marine sediments, many studies extrapolated permeabilities from fine-grained terrigenous sediments found on-shore, creating uncertainty in the results (e.g. Bryant et al., 1981). With the availability of more marine samples, the quantity of permeability data has significantly increased.

Previous studies based on permeability measurements from both marine and terrestrial sediments have suggested that correlation

* Corresponding author. Current address: Integrated Ocean Drilling Program, Texas A&M University, 1000, Discovery Drive, College Station, TX 77845, USA. Tel.: +1 979 862 2283; fax: +1 979 845 0876.
E-mail address: kusali@ufl.edu (K. Gamage).

0025-3227/$ – see front matter © 2010 Elsevier B.V. All rights reserved.
doi:10.1016/j.margeo.2010.10.010

between permeability and porosity could provide insight to a large range of sediments in nature (e.g. Neuzil, 1994; Bryant, 2002; Spinelli et al., 2004). Given the large variation in sediment permeability, it is necessary to use a systematic relationship between permeability and porosity to approximate the permeability structure in subduction zone fluid flow models (e.g. Saffer and Bekins, 1998). Similarly, lack of basic permeability–porosity relationships has greatly hampered the understanding of fluid flow and pressure generation in sedimentary basins (e.g. Alpin et al., 1999).

The primary purpose of this study is to synthesize available permeability data from the northern Barbados, Costa Rica, Nankai, and Peru subduction zones (Fig. 1 and Fig. S1) with the aim of defining and understanding permeability–porosity relationships. Here we developed permeability–porosity relationships based on sediment type and grain size distribution. Variations observed in permeability–porosity relationships were assessed based on the effect of interlayer water in smectite and the general compaction history.

2. Sampling locations

2.1. Barbados

The Barbados accretionary complex is formed where the North American Plate (Fig. S1a) is being subducted beneath the Caribbean Plate at a rate of about 2 cm a^{-1} in an east to west direction (DeMets et al., 1990). Active accretion of sediments at the Barbados accretionary complex takes place at the eastern end of the complex. At the location of DSDP and ODP drilling, the incoming sediments are predominantly clay and claystones. This study used core permeability measurements from ODP Leg 156 Sites 948 and 949 (Bruckmann et al., 1997; Zwart et al., 1997) and ODP Leg 110 Sites 671, 672, and 676 (Taylor and Leonard, 1990). The heat flow values at the drilled sites vary from 80 to 110 mW/m^2 and the thermal gradients vary from 66 to 97 °C/km (Shipboard Scientific Party, 1995a, b).

2.2. Costa Rica

The Middle American Trench (MAT) is formed by the eastward subduction of the Cocos Plate beneath the Caribbean Plate (Fig. S1b) at a rate of about 8.8 cm a^{-1} (Silver et al., 2000). Near the Nicoya Peninsula of Costa Rica, the incoming sedimentary sequence is about 380 m thick and consists of approximately 160 m of siliceous hemipelagic sediments overlying about 220 m of pelagic carbonates (Silver et al., 2000). Based on seismic reflection profiles and gamma ray logs, less than 5 m of sediments are being off-scraped at the toe of the margin, thus representing a nearly non-accretionary margin (Shipboard Scientific Party, 1997b). In this study we used core permeability measurements from ODP Leg 170, Sites 1039 and 1040 (Saffer et al., 2000; Screaton et al., 2006), and from ODP Leg 205, Sites 1253, 1254, and 1255 (McKiernan and Saffer, 2006; Screaton et al., 2006), including silty clays, diatom oozes, nannofossil chalks, and nannofossil oozes. Anomalously low heat flow values of ~13.5 mW/m^2 were measured in the trench (Langseth and Silver, 1996), increasing to 23.5 mW/m^2 landward of the frontal thrust and ~30 mW/m^2 farther upslope (Shipboard Scientific Party, 1997a). The average thermal gradient at Site 1039 is 9.6 °C/km (Shipboard Scientific Party, 1997b) and 7.2 °C/km at Site 1040 (Shipboard Scientific Party, 1997c).

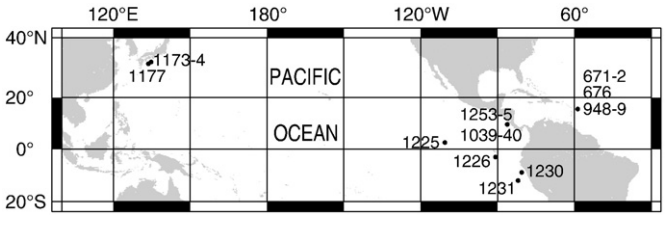

Fig. 1. Global location map showing drill sites where whole-round samples were taken for permeability measurements.

2.3. Nankai

The Nankai accretionary complex is formed by the subduction of the Philippine Sea Plate beneath the southwest Japan arc on the Eurasian Plate (Fig. S1c) at a rate of about 4 cm a^{-1} (Seno et al., 1993). The incoming sediments are predominantly composed of silty clays. Core permeability measurements presented in this study are from ODP Leg 190 Sites 1173, 1174 (Gamage and Screaton, 2003; Skarbek and Saffer, 2009), and 1177 (personal communication, T. Hays, 2005). Heat flow values range from 180 mW/m^2 at Sites 1173 and 1174 to 130 mW/m^2 at Site 808 (Shipboard Scientific Party, 2001b,c,d). The thermal gradients vary from 183 °C/km for Sites 1173/1174 (Shipboard Scientific Party, 2001b,c) to 60 °C/km at Site 1177 (Shipboard Scientific Party, 2001d).

2.4. Peru

The Peru accretionary complex is formed by the northeastward subduction at approximately 6.1 cm a^{-1} of the Nazca Plate (Hampel, 2002) below the Andean continental margin along the Peru Trench (Fig. S1d). This study used core permeability measurements from ODP Leg 201, Sites 1225, 1226, 1230, and 1231 (Gamage et al., 2005). These sites represent a wide range of subsurface environments in both open-ocean (Sites 1225, 1226, and 1231) and ocean-margin (Site 1230) provinces of the eastern tropical Pacific Ocean. Sediments vary from nannofossil oozes and chalks to diatom oozes. At the open-ocean sites, heat flow estimates vary from ~15 mW/m^2 at Site 1225 to ~49 mW/m^2 at Site 1226 and 51–64 mW/m^2 at Site 1231 (D'Hondt et al., 2003). At the ocean-margin Site 1230, estimated heat flow is 28 mW/m^2 (D'Hondt et al., 2003). The thermal gradient at Site 1225 is 7.4 °C/km (Shipboard Scientific Party, 2003a), at Site 1226 is 54 °C/km (Shipboard Scientific Party, 2003b), at Site 1230 is 34.3 °C/km (Shipboard Scientific Party, 2003c) and at Site 1231 it varies from 90 °C/km from 0–55 mbsf and 35 °C/km from 55–115 mbsf (Shipboard Scientific Party, 2003d).

3. Methods

3.1. Laboratory-measured permeability data

Laboratory-measured permeability data were provided by several sources for each of the four subduction zones. The two widely used methods for permeability measurements are direct flow tests (e.g., falling or constant head, constant-rate flow) and consolidation tests. Some studies have noted inconsistencies between calculated permeability values from consolidation tests and direct flow tests (Bryant et al., 1981; Taylor and Leonard, 1990; Zwart et al., 1997). Bryant et al. (1981) made a general observation that the permeability values computed from consolidation tests are one order of magnitude less than values obtained from direct measurements. A similar observation was made by Taylor and Leonard (1990) on ODP Leg 110 Barbados samples. In contrast, Zwart et al. (1997) found that permeability calculated using consolidation tests on Leg 156 (primarily claystone) samples generally overestimated direct measurement values and that the difference between the values for a given consolidation step varied from negligible up to a factor of 20. Saffer and McKiernan (2005), based on samples from Leg 205 (primarily clayey diatomite and diatom ooze), concluded that results between

the two methods were consistent. Although in general, consolidation tests are suitable for determining low permeability of fine-grained sediments, uncertainties linked to estimation of permeabilities from consolidation curves (e.g. difficulty in separating primary consolidation from secondary compression) could affect the estimated permeabilities. To minimize these uncertainties we constrain our data to only those obtained from direct flow measurements. Although this omits some Costa Rica data from McKiernan and Saffer (2006) and Nankai data from Skarbek and Saffer (2009), we note that these samples are represented in this study by their flow-through test results. We further limit our permeability measurement selection to those that have reported porosity or void ratio information. For consistency, only vertical permeabilities were used in this study; data on horizontal permeabilities are extremely limited. A brief explanation of methods used for permeability determination can be found in Appendix S1.

3.2. Sample selection and limitations

The data chosen for this study were obtained from homogeneous and coherent sections of whole-round cores preferentially selected to avoid large structural features such as faults. Even though the data used here include samples from structurally deformed regimes (e.g., accretionary prism, décollement), samples did not include scaly fabric and other deformational features that could provide dynamic flow paths or reduced permeability. Permeability values presented here therefore closely represent the matrix permeability of the sediment and exclude large-scale formation/fracture permeability.

Previous studies (e.g. Bolton and Maltman, 1998; Bolton et al., 2000) have shown that the largest decrease in permeability during sample testing occurs as effective stress increases from 0 to 100 kPa and subsequently, permeabilities remain relatively constant. We note that this observation applies only for effective stresses that do not exceed preconsolidation stress. Permeabilities used in this study were measured at varying effective stress values ranging from 20 to 1215 kPa (Table 1). In general, permeabilities decreased with increasing effective stress and deeper samples showed less variation with increase in effective stress. Overall, the maximum change of permeability is less than an order of magnitude over the range of test effective stress conditions. Many of the samples in this study were measured under confining pressures significantly less than in situ stress. By combining results from a variety of depths and testing conditions, we can assess whether this introduces anomalous values. If conducting the tests under stresses much less than in situ introduced significant error, we would not expect good relationships between permeability and porosity. Thus, in sediment types where we find good relationships between permeability and porosity, we feel confident that the introduced error by testing at effective stresses less than in situ is negligible. In contrast, where we do not see a good relationship, it is possible that there are artifacts introduced.

Grain alignment during consolidation can affect the tortuosity and, thus, permeability of sediments. However, Brown and Moore (1993) suggested that permeability increase by grain alignment is compensated by porosity decrease and by collapse of clay framework. In addition, several studies on natural and artificial clays suggest that the grain alignment does not increase significantly at loads over 250 kPa (e.g. Mcconnachie, 1974; Bennett et al., 1989; Clennell et al., 1999).

3.3. Permeability–porosity relationship

Bryant et al. (1975) and Neuzil (1994) observed that permeability of argillaceous sediments follows a log-linear relationship with porosity. The log-linear relationship is given by $\log(k) = \log(k_0) + bn$, where k_0 is the (fictitious) projected permeability at zero porosity, b is a fitting parameter, and n is the porosity. The coefficient of correlation (R^2) of the regression equation describes the variability of the estimates around the mean. However, the R^2 value inherits the problem of statistically small sample size. Thus, in such situations the derived statistics are not necessarily the best indicator of "goodness of fit".

3.4. Porosity correction for smectite

In clay-rich sediments where smectite is present, the existence of significant intragranular porosity can overestimate the intergranular porosity available for fluid flow. Smectite is a hydrated mineral that retains variable amounts of water in the interlayer region, and the amount of water retained is a function of temperature, pressure, interlayer cation species, and salinity (Colten-Bradley, 1987). The volumetric significance of interlayer water increases with burial (Brown and Ransom, 1996), and with increasing temperature and effective stress, the hydrated phase of smectite becomes unstable triggering the smectite–illite transformation, where illite is precipitated as a more stable diagenetic mineral.

The correction for smectite discussed in the following section is an attempt to calculate the intergranular porosity of clay-rich sediments (Table 1). We compared results with and without porosity corrections made following methods of Brown et al. (2001). For the correction, the mass fraction of interlayer water is assumed to be 0.20, corresponding to an interlayer spacing of 15 Å. This assumption was based on Brown et al. (2001) because smectite in contact with seawater may have an initial interlayer spacing of 18 Å at shallow burial depths, partially dehydrating to 15 Å as stress levels rise above ~1.5–3 MPa. It should be noted that samples used here may not represent depths reflecting stress levels of 1.5–3 MPa, and thus, using 15 Å spacing (mass fraction of 0.2) provides a conservative estimate of porosity related to interlayer water. However, at shallow depths (<1.5 km) and temperatures less than 60 °C, some of the interlayer water may have been released due to simple compaction (Colten-Bradley, 1987).

Smectite contents in the bulk sediment (Table 1) were available for all Nankai samples (Steurer and Underwood, 2003b) and some of the Barbados (Tribble, 1990; Underwood and Deng, 1997) and Peru samples (personal communication, M. Underwood, 2007). Weight percentage of smectite was calculated from X-ray diffraction (XRD) analyses of smectite relative percentage of clays and shipboard XRD clay relative percentage (Tribble, 1990; Shipboard Scientific Party, 1995a, b, 2001b, c, d). Values for Peru samples (except for Peru nannofossil ooze and chalk) were also determined using XRD smectite relative abundance and XRD relative clay abundance (personal communication, M. Underwood, 2007). Clay mineralogy data for Peru nannofossil oozes and chalks were unavailable to calculate corrected porosities.

Smectite content for clay-rich sediments from Costa Rica was established based on seafloor samples (Spinelli and Underwood, 2004) where clays averaged 87% smectite. This value is consistent with results for clay-rich ODP Leg 205 samples (Cardace, 2006). Absolute weight percentage of smectite averaged 60% (Spinelli and Underwood, 2004). Because data were unavailable for individual samples and smectite content for Costa Rica clay-rich sediments was observed to be relatively consistent (Spinelli and Underwood, 2004), this value (60%) was applied to all Costa Rica clay-rich samples. It should be noted that using seafloor samples at Costa Rica can overestimate smectite content at depth, as early diagenesis and overburden stress at shallow depths can release some of the interlayer water, as mentioned earlier. Costa Rica pelagic carbonates from Site 1253 had little clay minerals present in the samples (Cardace, 2006) and therefore the porosities were not affected by the porosity correction. Because this site is located along the same transect as Leg 170 Sites 1039 and 1040, it was assumed that pelagic carbonates from those sites are similar, and therefore porosity was unaffected by smectite interlayer water.

Table 1
Listing of permeability, porosity, grain size data, smectite, and clay percentages with references used in this study. † Grain size and carbonate data were assigned based on the grain size data available for similar samples from Screaton et al. (2006) for Costa Rica. *Represents samples used in the grain size classification. The following samples were excluded from lithologic classification due to lack of sufficient numbers of samples representing a lithological group or lithologic information was insufficient to assign to a group :170-1039B-10 H; 201-1231B-6 H, 3 H; 201-1225A-26 H; 110 (671B-3 H-3, 672A-5 H-3, 676A-2 H-3, 676A-5 H-3). # Where only hydraulic conductivity was provided, permeability was calculated using (Fetter, 1994), $k = K\mu/\rho g$, where k is intrinsic permeability [L2], K is hydraulic conductivity [L T−1], ρ is fluid density [M L−3], g is the gravitational constant [L T−2], and μ is the kinematic viscosity [M L−1 T−1]. Values of fluid density and viscosity were determined based on temperature values reported for the experiment and the salinity of the permeant used. In cases where temperature and/or permeant used were not reported, a temperature of 25 °C and a density (for the permeant) of 1023 kg/m^3 were assumed. Sample ID includes ODP site (hole) number and sequence, and the type of core barrel used: H = hydraulic piston core, X = extended core barrel, R = rotary core barrel, CC = core catcher.

Location	Permeability reference	Depth (mbsf)	Effective stress (kPa)	Permeability		Porosity	Permeant type	Structural domain	Lithology
				log k	(m^2)				
Barbados									
156-948 C-13X-3*	Vrolijk et al. (unpubl. data) in Zwart et al. (1997)	530.4	241	−18.31	4.90E−19	0.55	Saline	Underthrust	Gray claystone
156-949B-2X-1*	Maltman et al. (unpubl. data) in Zwart et al. (1997)	254.08	85	−17.33	4.70E−18	0.62	Fresh water	Prism	Gray to light gray-olive nannofossil-bearing claystone
			160	−17.35	4.50E−18	0.61			
			305	−17.78	1.66E−18	0.59			
			335	−17.79	1.64E−18	0.59			
			420	−17.84	1.45E−18	0.59			
			435	−17.89	1.30E−18	0.58			
			630	−17.87	1.36E−18	0.57			
			735	−18	1.00E−18	0.57			
			1215	−18.52	3.00E−19	0.56			
156-949B-15X-5*	Bruckmann et al. (1997)	366.23	192	−15.09	8.06E−16	0.7	Fresh water	Prism	Light olive-gray claystone
			384	−16.38	4.18E−17	0.69			
			768	−17.49	3.27E−18	0.69			
156-949B-19X-1*		399.2	96	−16.95	1.12E−17	0.62		Decollement	Yellowish brown radiolarian-bearing claystone
			192	−17.49	3.27E−18	0.62			
			384	−17.79	1.63E−18	0.61			
156-949B-22X-1*		428.75	192	−17.1	7.86E−18	0.55		Decollement	Light brownish gray radiolarian-bearing claystone
			384	−17.44	3.67E−18	0.55			
			768	−17.95	1.12E−18	0.54			
110-671B-3 H-3#	Taylor and Leonard (1990)	20.95	140	−15.99	1.02E−16	0.67	Not specified	Decollement	Calcareous mud
110-672A-5 H-3#		36.24	196	−17.44	3.60E−18	0.69		Reference site (incoming sediments)	Calcareous clay and mud
110-676A-2 H-3#		10.64	20	−17.51	3.09E−18	0.73		Deformation front site	Calcareous mud
110-676A-5 H-3#		39.12	33	−16.99	1.02E−17	0.75		Deformation front site	Calcareous mud
Nankai									
190-1173A-22 H-2*	Gamage and Screaton (2003)	199.9	240	−16.29	5.18E−17	0.57	Seawater	Reference site (incoming sediments)	Silty clay
			420	−16.39	4.05E−17	0.56			
			540	−16.41	3.92E−17	0.55			
190-1173A-31X-1*		284.59	270	−16.7	1.99E−17	0.62		Reference site (incoming sediments)	Silty claystone to clayey siltstone
			420	−16.89	1.29E−17	0.6			
190-1173A-39X-5*		367.07	260	−17.61	2.48E−18	0.41		Reference site (incoming sediments)	Silty claystone
			390	−17.66	2.19E−18	0.36			
			550	−17.82	1.52E−18	0.33			
190-1173A-41X-CC*		388.75	290	−17.6	2.50E−18	0.45		Reference site (incoming sediments)	Silty claystone, mottled
			410	−17.78	1.67E−18	0.43			
			550	−17.93	1.18E−18	0.43			
190-1173A-46X-1*		428.59	250	−17.72	1.91E−18	0.45		Reference site (incoming sediments)	Silty claystone
			400	−17.82	1.53E−18	0.43			
			510	−17.9	1.25E−18	0.41			
190-1174B-42R-3*		538.23	190	−17.1	7.89E−18	0.37		Prism	Silty claystone, altered ash
			480	−17.7	2.01E−18	0.34			
			620	−17.82	1.53E−18	0.32			
190-1174B-59R-5*		704.95	270	−18.28	5.22E−19	0.32		Prism	Silty claystone
			410	−18.45	3.55E−19	0.3			
			550	−18.53	2.96E−19	0.28			
190-1174B-69R-2*		795.17	270	−18.07	8.54E−19	0.29		Prism	Silty claystone
			410	−18.24	5.82E−19	0.28			
			550	−18.54	2.85E−19	0.26			
190-1174B-74R-1*		842.75	270	−18.19	6.44E−19	0.3		Underthrust	Silty claystone
			410	−18.21	6.20E−19	0.28			
			550	−18.32	4.74E−19	0.27			
190-1177A-25R-2*	Hays (University of Florida, personal communication, 2005)	533.2	414	−17.79	1.63E−18	0.45	Seawater	Reference site (incoming sediments)	Silty claystone
			620	−17.97	1.07E−18	0.42			
			827	−18.09	8.22E−19	0.4			

Grain size (wt.%)			Carbonate (wt.%)	Grain size and carbonate (wt.%) reference	Calculations based on phyllosilicate (clay mineral) content						
Sand (>63 μm)	Silt (63–4 μm)	Clay (<4 μm)			Smectite (% of clay)	Smectite reference	Clay %	Clay reference	Calculated smectite (% of solids)	Smectite % reference	Corrected porosity
0	8	92	0	Meyer and Fisher (1997)	19	Underwood and Deng, 1997	75.1	Shipboard Scientific Party, 1995a	14.3		0.51
0	9	91	9.9	Meyer and Fisher (1997)	30	Underwood and Deng, 1997	64.6	Shipboard Scientific Party, 1995b	19.4		0.57
0	9	91	9.9						19.4		0.56
0	9	91	9.9						19.4		0.54
0	9	91	9.9						19.4		0.54
0	9	91	9.9						19.4		0.54
0	9	91	9.9						19.4		0.52
0	9	91	9.9						19.4		0.51
0	9	91	9.9						19.4		0.51
0	9	91	9.9						19.4		0.50
0	9	91	0	Meyer and Fisher (1997)	70	Underwood and Deng, 1997	60.6	Shipboard Scientific Party, 1995b	42.4		0.61
0	9	91							42.4		0.60
0	9	91							42.4		0.60
3	12	85	0	Meyer and Fisher (1997)	43	Underwood and Deng, 1997	63.0	Shipboard Scientific Party, 1995b	27.1		0.55
3	12	85							27.1		0.55
3	12	85							27.1		0.54
1	7	92	0	Meyer and Fisher (1997)	30	Underwood and Deng, 1997	65.7	Shipboard Scientific Party, 1995b	19.7		0.49
1	7	92							19.7		0.49
1	7	92							19.7		0.48
			38.7	Taylor and Leonard (1990)	29	Tribble (1990)	27.0	Tribble (1990)	7.8		0.65
			48.6	Taylor and Leonard (1990)	28	Tribble (1990)	42.0	Tribble (1990)	11.8		0.67
			30.1	Taylor and Leonard (1990)							
			18.6	Taylor and Leonard (1990)							
1	48	51	3.56	Steurer and Underwood (2003a); Shipboard Scientific Party, 2001b	35.6	Steurer and Underwood (2003b)	42.0	Shipboard Scientific Party (2001b)	14.9		0.53
1	48	51							14.9		0.52
1	48	51							14.9		0.50
2	39	59	5.94	Steurer and Underwood (2003a); Shipboard Scientific Party, 2001b	46.2	Steurer and Underwood (2003b)	48.0	Shipboard Scientific Party (2001b)	22.2		0.56
2	39	59							22.2		0.54
1	55	44	2.45	Steurer and Underwood (2003a); Shipboard Scientific Party, 2001b	63.4	Steurer and Underwood (2003b)	55.0	Shipboard Scientific Party (2001b)	34.9		0.27
1	55	44							34.9		0.21
1	55	44							34.9		0.17
1	51	48	1.4	Steurer and Underwood (2003a); Shipboard Scientific Party, 2001b	64.3	Steurer and Underwood (2003b)	54.0	Shipboard Scientific Party (2001b)	34.7		0.32
1	51	48							34.7		0.30
1	51	48							34.7		0.30
0	31	69	1.12	Steurer and Underwood (2003a); Shipboard Scientific Party, 2001b	48.0	Steurer and Underwood (2003b)	57.0	Shipboard Scientific Party (2001b)	27.3		0.35
0	31	69							27.3		0.32
0	31	69							27.3		0.30
1	44	56	1.54	Steurer and Underwood (2003a); Shipboard Scientific Party, 2001c	43.6	Steurer and Underwood (2003b)	52.0	Shipboard Scientific Party (2001c)	22.7		0.27
1	44	56							22.7		0.24
1	44	56							22.7		0.22
1	32	68	0.96	Steurer and Underwood (2003a); Shipboard Scientific Party, 2001c	53.1	Steurer and Underwood (2003b)	49.0	Shipboard Scientific Party (2001c)	26.0		0.20
1	32	68							26.0		0.18
1	32	68							26.0		0.15
1	37	62	1.75	Steurer and Underwood (2003a); Shipboard Scientific Party, 2001c	36.8	Steurer and Underwood (2003b)	52.0	Shipboard Scientific Party (2001c)	19.2		0.20
1	37	62							19.2		0.19
1	37	62							19.2		0.16
0	26	74	33.36	Steurer and Underwood (2003a); Shipboard Scientific Party, 2001c	30.5	Steurer and Underwood (2003b)	26.0	Shipboard Scientific Party (2001c)	7.9		0.26
0	26	74							7.9		0.24
0	26	74							7.9		0.23
0	30	70	0.65	Steurer and Underwood (2003a); Shipboard Scientific Party, 2001d	47.5	Steurer and Underwood (2003b)	56.0	Shipboard Scientific Party (2001d)	26.6		0.35
0	30	70							26.6		0.32
0	30	70							26.6		0.29

(continued on next page)

Table 1 (*continued*)

Location	Permeability reference	Depth (mbsf)	Effective stress (kPa)	Permeability log k (m^2)		Porosity	Permeant type	Structural domain	Lithology
Nankai									
190-1177A-46R-2	Hays (University of Florida, personal communication, 2005)	732.54	689	−17.81	1.54E−18	0.37		Reference site (incoming sediments)	Silty claystone
			827	−18.29	5.15E−19	0.36			
190-1173A-12 H-4*	Skarbek and Saffer (2009)	107.14	1324	−16.57	2.72E−17	0.61		Reference site (incoming sediments)	Silty clay
		107.14	3563	−16.93	1.17E−17	0.58		Reference site (incoming sediments)	Silty clay
		107.14	6186	−17.34	4.56E−18	0.54		Reference site (incoming sediments)	Silty clay
		107.14	12386	−17.82	1.50E−18	0.51		Reference site (incoming sediments)	Silty clay
190-1173A-24 H-1*	Skarbek and Saffer (2009)	217.44	7028	−17.16	6.95E−18	0.43		Reference site (incoming sediments)	Silty clay
190-1173A-49X*	Skarbek and Saffer (2009)	464.71	817	−18.11	7.78E−19	0.4		Reference site (incoming sediments)	Silty claystone
		464.71	1224	−18.23	5.94E−19	0.39		Reference site (incoming sediments)	Silty claystone
		464.71	7008	−18.97	1.06E−19	0.31		Reference site (incoming sediments)	Silty claystone
Costa Rica									
170-1039B-10 H-2	Saffer et al. (2000)	80.85		−16.4	3.98E−17	0.62		Reference site (incoming sediments)	Diatom ooze/silty-clay with ash layers
				−16.4	3.98E−17	0.68			
				−16	1.00E−16	0.75			
				−15.9	1.26E−16	0.75			
170-1039B-16X-8		141.54		−17.6	2.51E−18	0.67		Reference site (incoming sediments)	Silty clay with calcareous clay, ash layers
				−17.1	7.94E−18	0.68			
				−16.4	3.98E−17	0.76			
				−15.5	3.16E−16	0.79			
				−14.8	1.58E−15	0.8			
170-1039B-26X-6		237.25		−15.5	3.16E−16	0.53		Reference site (incoming sediments)	Nannofossil ooze
				−15.2	6.31E−16	0.56			
				−15.3	5.01E−16	0.58			
				−15	1.00E−15	0.59			
				−14.8	1.58E−15	0.61			
				−14.2	6.31E−15	0.62			
170-1040 C-30R-4		442.7		−15.1	7.94E−16	0.79		Underthrust	Silty claystone with ash layers
				−15.8	1.58E−16	0.78			
				−16.8	1.58E−17	0.69			
				−16.9	1.26E−17	0.72			
205-1253A-2R-4	McKiernan and Saffer (2006)	380.07		−15.99	1.03E−16	0.46	Freshwater	Reference site (incoming sediments)	Nannofossil chalk with diatoms
205-1253A-3R-2		386.83		−16.3	5.07E−17	0.5		Reference site (incoming sediments)	Nannofossil chalk with diatoms
205-1253A-4R-1		394.91		−16.9	1.25E−17	0.47		Reference site (incoming sediments)	Nannofossil chalk with diatoms
205-1254A-16R-4		366.74		−18.58	2.62E−19	0.39		Decollement	Clayey diatomite with ash layers and silty sand
205-1255A-2R-CC*		134.89		−19.03	9.25E−20	0.32		Underthrust	Silty clay and breccia
				−15.32	4.81E−16	0.50			
				−17.1	7.86E−18	0.47			
				−17.82	1.52E−18	0.44			
				−18.34	4.57E−19	0.39			
				−18.83	1.49E−19	0.32			
205-1255A-3R-CC*		146.48		−19.02	9.55E−20	0.41		Underthrust	Diatom Ooze
205-1255A-4R-CC*		152.38		−19.12	7.66E−20	0.26		Underthrust	Diatom Ooze
				−17.01	9.76E−18	0.65			
				−17.07	8.50E−18	0.65			
				−17.79	1.63E−18	0.57			
170-1040 C-38R-2	Screaton et al. (2006)	518	140	−14.88	1.31E−15	0.57	Seawater	Underthrust	Siliceous nannofossil chalk
			480	−14.92	1.20E−15	0.55			
			620	−14.97	1.07E−15	0.54			

Grain size (wt.%)			Carbonate (wt.%)	Grain size and carbonate (wt.%) reference	Calculations based on phyllosilicate (clay mineral) content						
Sand (>63 μm)	Silt (63–4 μm)	Clay (<4 μm)			Smectite (% of clay)	Smectite reference	Clay %	Clay reference	Calculated smectite (% of solids)	Smectite % reference	Corrected porosity
38	27	32	1	Steurer and Underwood (2003a); Shipboard Scientific Party, 2001d	75.3	Steurer and Underwood (2003b)	41.0	Shipboard Scientific Party (2001d)	30.9		0.24
38	27	32							30.9		0.23
3	74	23	0.92	Steurer and Underwood (2003a); Shipboard Scientific Party, 2001b	22	Steurer and Underwood (2003a)	47.0	Shipboard Scientific Party (2001b)0	10.0		0.58
3	74	23	0.92						10.0		0.55
3	74	23	0.92						10.0		0.51
3	74	23	0.92						10.0		0.48
4	41	56	8.25	Steurer and Underwood (2003a); Shipboard Scientific Party, 2001b	48		40.0	Shipboard Scientific Party (2001b)	19.0		0.36
0	31	69	0.75	Steurer and Underwood (2003a); Shipboard Scientific Party, 2001b	43		56.0	Shipboard Scientific Party (2001b)	24.0		0.30
0	31	69	0.75						10.0		0.35
0	31	69	0.75						10.0		0.26
		†51	4.67	Screaton et al. (2006)					60	Spinelli and	0.47
		†51	4.67						60	Underwood	0.55
		†51	4.67						60	(2004)	0.65
		†51	4.67						60		0.65
		†51	4.67	Screaton et al. (2006)					60	Spinelli and	0.54
		†51	4.67						60	Underwood	0.55
		†51	4.67						60	(2004)	0.66
		†51	4.67						60		0.70
		†51	4.67						60		0.72
							0.0	Cardace (2006)			0.53
							0.0				0.56
							0.0				0.58
							0.0				0.59
							0.0				0.61
							0.0				0.62
		†51	4.67	Screaton et al. (2006)					60	Spinelli and	0.70
		†51	4.67						60	Underwood	0.69
		†51	4.67						60	(2004)	0.56
		†51	4.67						60		0.61
†1	49	50	57.41	Screaton et al. (2006)			0.0	Cardace (2006)			0.46
†2	43	55	47.41	Screaton et al. (2006)			0.0	Cardace (2006)			0.5
†8	50	42	_	Screaton et al. (2006)			0.0	Cardace (2006)			0.47
†6	39	55	1.43	Screaton et al. (2006)					60	Spinelli and Underwood (2004)	0.14
†3	46	51	4.67	Screaton et al. (2006)					60	Spinelli and	0.04
†3	46	51	4.67						60	Underwood	0.30
†3	46	51	4.67						60	(2004)	0.26
†3	46	51	4.67						60		0.21
†3	46	51	4.67						60		0.14
†3	46	51	4.67						60		0.04
†1	34	65	1.59	Screaton et al. (2006)					60	Spinelli and Underwood (2004)	0.17
†1	34	65	1.77	Screaton					60	Spinelli and	-0.04
†1	34	65	1.77	et al. (2006)					60	Underwood	0.51
†1	34	65	1.77						60	(2004)	0.50
†1	34	65	1.77						60		0.39
1	54	46	89.66	Screaton et al. (2006)			0.0	Cardace (2006)			0.57
1	54	46	89.66				0.0				0.55
1	54	46	89.66				0.0				0.54

(continued on next page)

Table 1 (*continued*)

Location	Permeability reference	Depth (mbsf)	Effective stress (kPa)	Permeability log k (m^2)		Porosity	Permeant type	Structural domain	Lithology
Costa Rica									
170-1040 C-46R-4		598	140	−15	1.01E−15	0.6		Underthrust	Nannofossil chalk, diatomite and breccia
			480	−15.04	9.12E−16	0.59			
			620	−15.05	8.86E−16	0.58			
205-1253A-02R-3		379	140	−15.17	6.83E−16	0.66		Reference site (incoming sediments)	Nannofossil chalk with diatoms
			480	−15.23	5.95E−16	0.64			
			620	−15.27	5.42E−16	0.62			
205-1253A-03R-1		386	140	−15.02	9.60E−16	0.71		Reference site (incoming sediments)	Nannofossil chalk with diatoms
			480	−15.27	5.43E−16	0.69			
			620	−15.39	4.10E−16	0.67			
205-1255A-02R-CC*		135	140	−17.51	3.07E−18	0.57		Underthrust	Silty clay and breccia
			480	−17.62	2.39E−18	0.56			
			620	−17.77	1.69E−18	0.53			
205-1255A-03R-CC*		147	140	−17.76	1.75E−18	0.49		Underthrust	Diatom oozes
			480	−17.76	1.74E−18	0.47			
			620	−17.79	1.64E−18	0.46			
205-1255A-04R-CC*		152	140	−17.44	3.61E−18	0.66		Underthrust	Diatom oozes
			480	−17.52	3.00E−18	0.64			
			620	−17.64	2.28E−18	0.59			
Peru									
201-1231B-3 H	Gamage et al. (2005)	17.1	140	−16.5	3.14E−17	0.89	Seawater	Peru Basin	Diatom-rich clay
			270	−16.99	1.02E−17	0.87			
			410	−17.17	6.77E−18	0.86			
			550	−17.46	3.44E−18	0.85			
201-1231B-6 H		44.1	140	−15.83	1.49E−16	0.85		Peru Basin	Volcanic glass-rich clay
			270	−16.27	5.36E−17	0.83			
			410	−16.6	2.49E−17	0.82			
			550	−16.82	1.51E−17	0.8			
201-1231B-9 H		75.7	140	−15.11	7.75E−16	0.59		Peru Basin	Nannofossil ooze
			270	−15.25	5.66E−16	0.58			
			410	−15.34	4.55E−16	0.57			
			550	−15.37	4.26E−16	0.56			
201-1231B-13 H		112.1	140	−15.33	4.63E−16	0.66		Peru Basin	Nannofossil ooze
			270	−15.39	4.09E−16	0.65			
			410	−15.42	3.78E−16	0.64			
			550	−15.44	3.66E−16	0.63			
201-1230A-4 H*		31	140	−16.73	1.85E−17	0.680		Lower slope of Peru trench	Clay-rich diatom ooze
			270	−16.77	1.70E−17	0.670			
			410	−16.89	1.30E−17	0.660			
			550	−16.94	1.15E−17	0.640			
201-1230A-9 H		70.7	140	−16.24	5.75E−17	0.68		Lower slope of Peru trench	Clay-rich diatom ooze
			270	−16.37	4.24E−17	0.68			
			410	−16.47	3.39E−17	0.67			
			550	−16.51	3.09E−17	0.67			
201-1230A-31X*		230.8	140	−16.48	3.32E−17	0.53		Lower slope of Peru trench	Clay and quartz rich diatom ooze and diatom-rich siliciclastic
			270	−16.71	1.94E−17	0.49			
			410	−16.79	1.63E−17	0.48			
			550	−16.83	1.47E−17	0.45			
201-1230A-35X*		252.1	140	−16.69	2.02E−17	0.58		Lower slope of Peru trench	Clay and quartz rich diatom ooze and diatom-rich siliciclastic
			270	−16.75	1.79E−17	0.55			
			410	−16.85	1.41E−17	0.53			
			550	−16.9	1.25E−17	0.51			
201-1226B-4 H		24.8	140	−15.17	6.77E−16	0.76		Equatorial Pacific	Diatom-rich nannofossil oozes
			270	−15.27	5.36E−16	0.74			
			410	−15.33	4.69E−16	0.73			
			550	−15.37	4.24E−16	0.73			
201-1226B-26 H		239.6	140	−15.52	3.04E−16	0.67		Equatorial Pacific	Diatom-rich nannofossil oozes
			270	−15.51	3.06E−16	0.67			
			410	−15.53	2.92E−16	0.66			
			550	−15.54	2.86E−16	0.65			

Grain size (wt.%)			Carbonate (wt.%)	Grain size and carbonate (wt.%) reference	Calculations based on phyllosilicate (clay mineral) content						
Sand (>63 μm)	Silt (63–4 μm)	Clay (<4 μm)			Smectite (% of clay)	Smectite reference	Clay %	Clay reference	Calculated smectite (% of solids)	Smectite % reference	Corrected porosity
1	58	41	69.75	Screaton et al. (2006)			0.0	Cardace (2006)			0.6
1	58	41	69.75				0.0				0.59
1	58	41	69.75				0.0				0.58
1	49	50	57.41	Screaton et al. (2006)			0.0	Cardace (2006)			0.66
1	49	50	57.41				0.0				0.64
1	49	50	57.41				0.0				0.62
2	43	55	47.41	Screaton et al. (2006)			0.0	Cardace (2006)			0.71
2	43	55	47.41				0.0				0.69
2	43	55	47.41				0.0				0.67
3	46	51	4.67	Screaton et al. (2006)					60	Spinelli and	0.40
3	46	51	4.67						60	Underwood	0.38
3	46	51	4.67						60	(2004)	0.34
1	34	65	1.59	Screaton et al. (2006)					60	Spinelli and	0.28
1	34	65	1.59						60	Underwood	0.25
1	34	65	1.59						60	(2004)	0.24
1	34	65	1.77	Screaton et al. (2006)					60	Spinelli and	0.52
1	34	65	1.77						60	Underwood	0.49
1	34	65	1.77						60	(2004)	0.42
				Aiello (Moss Landing Marine Laboratories, personal communication, 2005)					37.8	Underwood (University of Missouri, personal communication, 2007)	0.86
									37.8		0.84
									37.8		0.82
									37.8		0.81
30	63	7		Aiello (Moss Landing Marine Laboratories, personal communication, 2005)							
30	63	7									
30	63	7									
30	63	7									
0	55	45		Aiello (Moss Landing Marine Laboratories, personal communication, 2005)							
0	55	45									
0	55	45									
0	55	45									
0	59	41		Aiello (Moss Landing Marine Laboratories, personal communication, 2005)							
0	59	41									
0	59	41									
0	59	41									
0	56	44							14.7	Underwood (University of Missouri, personal communication, 2007)	0.65
0	56	44							14.7		0.64
0	56	44							14.7		0.63
0	56	44							14.7		0.60
9	77	14							9.2	Underwood (University of Missouri, personal communication, 2007)	0.66
9	77	14							9.2		0.66
9	77	14							9.2		0.65
9	77	14							9.2		0.65
2	72	26		Aiello (Moss Landing Marine Laboratories, personal communication, 2005)					17.4	Underwood (University of Missouri, personal communication, 2007)	0.47
2	72	26							17.4		0.43
2	72	26							17.4		0.42
2	72	26							17.4		0.39
0	38	62		Aiello (Moss Landing Marine Laboratories, personal communication, 2005)					35.7	Underwood (University of Missouri, personal communication, 2007)	0.48
0	38	62							35.7		0.44
0	38	62							35.7		0.42
0	38	62							35.7		0.39
0	53	47		Aiello and Kellett (2006)							
0	53	47									
0	53	47									
0	53	47									
				Aiello and Kellett (2006)							

(continued on next page)

Table 1 (*continued*)

Location	Permeability reference	Depth (mbsf)	Effective stress (kPa)	Permeability log k	(m^2)	Porosity	Permeant type	Structural domain	Lithology
Peru									
201-1226B-43X		381.2	140	−16.8	1.57E−17	0.62		Equatorial Pacific	Diatom-bearing nannofossil chalk
			270	−16.85	1.40E−17	0.58			
			410	−16.91	1.24E−17	0.57			
			550	−16.99	1.02E−17	0.56			
201-1226B-46X		409.4	140	−17.73	1.85E−18	0.58		Equatorial Pacific	Nannofossil chalk
			270	−17.85	1.41E−18	0.56			
			410	−17.88	1.33E−18	0.53			
			550	−17.9	1.25E−18	0.52			
201-1225A-4 H		24.7	140	−15.44	3.61E−16	0.78		Equatorial Pacific	Diatom-rich nannofossil ooze
			270	−15.55	2.82E−16	0.75			
			410	−15.79	1.63E−16	0.73			
			550	−15.7	1.99E−16	0.71			
201-1225A-10 H		83.2	140	−15.62	2.41E−16	0.68		Equatorial Pacific	Diatom-rich nannofossil ooze
			270	−15.68	2.11E−16	0.66			
			410	−15.77	1.69E−16	0.65			
			550	−15.84	1.43E−16	0.64			
201-1225A-26 H		242.7	140	−15.17	6.78E−16	0.68		Equatorial Pacific	Nannofossil-rich diatom ooze
			270	−15.22	6.01E−16	0.66			
			410	−15.28	5.24E−16	0.65			
			550	−15.35	4.49E−16	0.64			
201-1225A-34 H		309.7	140	−15.63	2.37E−16	0.64		Equatorial Pacific	Diatom-bearing nannofossil chalk
			270	−15.66	2.19E−16	0.63			
			410	−15.72	1.90E−16	0.62			
			550	−15.74	1.81E−16	0.61			

3.5. Grain size classification

Grain size is a key factor that controls pore size distribution (Dewhurst et al., 1999), and it is the most important characteristic of a sediment in determining permeability (Bryant et al., 1981). Siliciclastic rocks composed predominantly of clay- and silt-sized particles can have permeabilities varying as much as by 10 orders of magnitude, spanning a range of three orders of magnitude at a single porosity (Dewhurst et al., 1999). According to Dewhurst et al. (1999) much of this variation can be related to grain size. However, a study by Koltermann and Gorelick (1995) suggests that grain size distribution has very little effect on permeability once the clay fraction is greater than 40%.

In order to understand the general trend of permeability–porosity relationships based on grain size distribution, we subdivided the data using Bryant's (2002) groupings for Gulf of Mexico sediments.

Group 1, sediment containing more than 80% clay-size material.

Group 2, sediment containing 60% to 80% clay-size material.

Group 3, sediment containing silty clays with less than 60% clay-size material and less than 5% sand.

Group 4, sediment containing sandy silts with less than 60% clay-size material and more than 5% sand.

The following particle size criteria were used for classification: sand (>63 μm), silt (4–63 μm) and clay (<4 μm). The grain size percentage refers to absolute wt.% values given in Table 1. It should be noted that in the grain size classification the term "clay" refers to particle size and is applied to any sediment particle regardless of its mineralogical composition. In order to understand the general trend of permeability–porosity relationships based on grain size distribution, we compared the subduction zone data with Bryant's (2002) relationships for Gulf of Mexico permeabilities.

Bryant (2002) noted that low amounts of carbonate had no effect on the permeability–porosity relationship of fine-grained marine sediments. However, the percent of carbonate that was considered low was not specified; thus, here we used 50 wt.% $CaCO_3$ as the cut off value. The cutoff value was used primarily because the majority of the calcareous pelagic samples contained either distinctively high (>>50 wt.% $CaCO_3$) or low (<<50 wt.% $CaCO_3$) amounts of $CaCO_3$. For samples that did not have $CaCO_3$ wt.% data, we used information from other methods such as XRD and inorganic carbon percentages to infer whether samples were likely to contain greater than 50 wt.% carbonates. All samples used in the grain size classification (marked with an asterisk) and values of available weight percentages of $CaCO_3$ are included in Table 1.

3.6. Classification of deep-sea sediments

There is little agreement regarding the classification of deep-sea sediments. Suggested classifications range from those that are largely genetic to those that are largely descriptive (e.g. Boggs, 2001). Unfortunately, there is no single classification that takes into account both genesis and descriptive properties for all kinds of deep-sea sediments (Boggs, 2001). To be consistent with the ODP lithological descriptions applied to samples by other workers, we used a commonly used ODP descriptive classification scheme based on Mazzullo et al. (1988), with several simplifying modifications for sediments that are mixtures of siliciclastic and biogenic components. Based on this classification, if the total siliciclastic content is >60%, the main name is determined by the relative proportions of sand, silt, and clay sizes (i.e., silty claystone). If the total biogenic content is >60% (i.e., siliciclastic material <40%), then the principal name applied is ooze or chalk (i.e., diatom ooze, nannofossil ooze or chalk). Oozes represent unconsolidated calcareous and/or siliceous biogenic sediment and chalks represent semi-indurated biogenic sediment composed predominantly of calcareous biogenic grains. For nonbiogenic clastic sediments, the two classes of induration are soft (i.e., silt, clay) and hard (i.e., siltstone, claystone). The detailed classification scheme can be found in Shipboard Scientific Party (2003a).

Based on this classification scheme, samples from northern Barbados and Nankai were grouped as siliciclastic sediments. Samples

Grain size (wt.%)			Carbonate (wt.%)	Grain size and carbonate (wt.%) reference	Calculations based on phyllosilicate (clay mineral) content						
Sand (>63 μm)	Silt (63–4 μm)	Clay (<4 μm)			Smectite (% of clay)	Smectite reference	Clay %	Clay reference	Calculated smectite (% of solids)	Smectite % reference	Corrected porosity
0	51	49		Aiello and Kellett (2006)							
0	51	49									
0	51	49									
0	51	49									
12	66	22		Aiello and Kellett (2006)							
12	66	22									
12	66	22									
12	66	22									
8	75	17		Aiello and Kellett (2006)							
8	75	17									
8	75	17									
8	75	17									
0	64	36		Aiello and Kellett (2006)							
0	64	36									
0	64	36									
0	64	36									
0	69	31		Aiello and Kellett (2006)							
0	69	31									
0	69	31									
0	69	31									
7	80	13		Aiello and Kellett (2006)							
7	80	13									
7	80	13									
7	80	13									

from Costa Rica consist of both siliciclastic and biogenic sediments. Peru samples consist only of biogenic sediments. Peru samples from Sites 1225 and 1226 represent undeformed equatorial Pacific sediments; thus, they do not strictly belong to the Peru subduction zone. However, these samples predominantly consist of nannofossil oozes and nannofossil chalk and thus can be compared to nannofossil oozes and chalks of Costa Rica, and for that purpose they were included in this study.

4. Results

The majority of permeability values were enveloped within Neuzil's (1994) plot of permeabilities as a function of porosity for argillaceous sediments before porosity was corrected for smectite (Fig. 2a). Several biogenic sediment samples from Site 1231 off Peru and Sites 1039 and 1040 off Costa Rica plotted outside Neuzil's (1994) area.

4.1. Effect of porosity correction for smectite

After correction for smectite (Fig. 2b), the entire data set shifted toward lower porosities except for those samples that do not contain clay minerals. A considerable number of samples from Costa Rica and Nankai moved out of Neuzil's (1994) envelope after the correction because Neuzil's compilation uses uncorrected porosity values. Use of a single smectite percentage for Costa Rica results in a negative porosity value for one test, likely reflecting error in the estimated smectite percentage (Table 1). Although smectite-corrected porosities are more appropriate when formulating porosity-permeability relations for clay-rich sediments, here we present both corrected and uncorrected porosities for two main reasons: (1) we were unable to perform smectite correction for all the samples presented in this study due to lack of data, and (2) most published porosity data and permeability–porosity compilations (e.g. Neuzil, 1994; Bryant, 2002; Spinelli et al., 2004) are not corrected for smectite, and therefore uncorrected porosities are useful in comparative studies.

4.2. Effects of grain size

Following the grain size classification described by Bryant (2002), the log-linear relationships obtained by least-squares regression fit are given in Table 2 for Groups 1 (>80% clay-size material) to 3 (<60% clay-size material and <5% sand). Group 4 (<60% clay-size material and >5% sand) was excluded, as it only contained a total of eight samples, predominantly from Peru. The permeability–porosity relationships obtained from grain size classification show a general trend where permeability increases with decreasing percentage of clay size particles at a given porosity (Fig. 3a, b).

We used the uncorrected porosities for comparison with Bryant's (2002) data, as those data were not corrected for any smectite present in the samples. Despite the differences in location, the grain size data from this study fall in the same general region predicted by Bryant (2002). For Group 1, the predicted permeabilities from this study are consistent with the permeabilities of Bryant (2002) at porosities around 0.7. As porosities decrease, our relationship for Group 1 predicts lower values of permeability than Bryant's (2002) permeability–porosity relationship. Groups 2 and 3 represent a larger range of porosities, between approximately 0.25 and 0.70, than available for Group 1. Both Groups 2 and 3 cross Bryant's (2002) permeability–porosity relationship at porosity of 0.5. Although grain size classification results using corrected porosities could not directly be compared to those of Bryant (2002), corrected porosities improved the correlation between permeability and porosity for Groups 2 and 3 (Table 2).

4.3. Effects of lithologic grouping

Overall, siliciclastic sediments yield a wide range of permeabilities, varying from 10^{-19} to 10^{-14} m^2 for uncorrected porosity values from

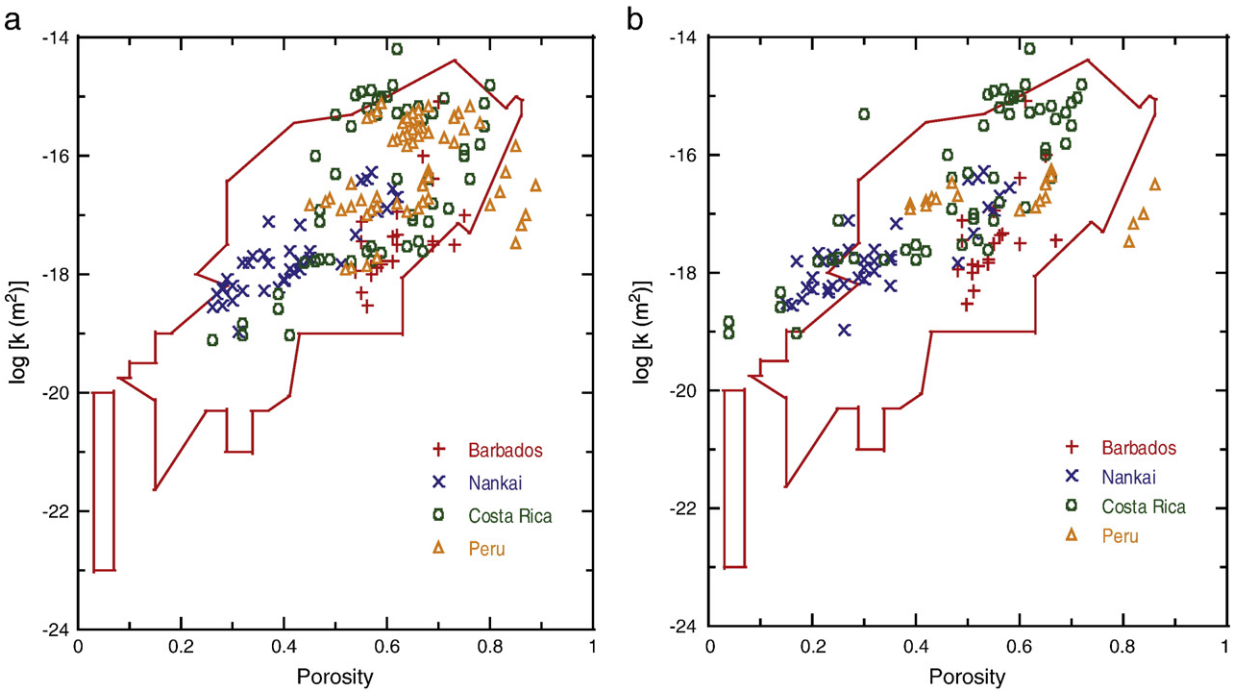

Fig. 2. Plot of laboratory-derived permeability measurements as a function of porosity from Barbados, Costa Rica, Nankai, and Peru subduction zones superimposed on outline of Neuzil (1994) plot for argillaceous sediments. As compared to Neuzil (1994) paper, the axes have been transposed. a) Using uncorrected porosity. b) Using corrected porosity.

0.3 to 0.8 and for corrected porosities from 0.15 to 0.7 (Fig. 4a, b and Table 3). All siliciclastic sediments were subcategorized as claystone and silty claystone. Both siliciclastic subgroups exhibit the same general trend when either uncorrected or corrected porosity values are considered (Fig. 4a, b). The correlation for Barbados claystones decreased by 37%, when corrected porosities were used. This poor correlation is likely related to the statistically small sample size in this group.

For biogenic sediments, the diatom oozes plot within the values of siliciclastic sediments for corrected porosities of 0.15–0.7 (uncorrected porosities of 0.25–0.7) with permeability values ranging from 10^{-19} to 10^{-16} (Fig. 5a, b and Table 3). The diatom ooze porosity values are more similar to the values of silty claystones than to those of claystones. Essentially, the trends for diatom oozes are identical to overall siliciclastics for both corrected and uncorrected porosities. The correlation between permeability and porosity for this group increased by 16% when corrected porosity was used.

Nannofossil oozes and chalks show a low correlation between permeability and porosity (Fig. 5c and Table 3). The porosity for both groups varies from ~0.4 to 0.8. The permeabilities for nannofossil oozes vary between 10^{-16} and 10^{-14} m^2, which is approximately 1.5 orders of magnitude higher than siliciclastic sediments (Fig. 5c). The nannofossil chalks have a wider range of permeabilities (10^{-18} m^2 to 10^{-15}), and the upper values overlap nannofossil ooze permeabilities while the lower values overlap siliciclastic permeabilities.

5. Discussion

5.1. Smectite correction

Uncorrected porosities of the siliciclastic samples used in this study fall within the area of Neuzil's (1994) plot of argillaceous sediments but shift out of the plot toward lower porosities when smectite-corrected porosities were used. In most cases, smectite-corrected porosities removed scatter observed in the permeability–porosity relationship and lowered porosities as much as by 0.16 (excluding Costa Rica samples). These results clearly suggest the need for better defined and routinely measured smectite data and demonstrate the value of a more standardized way of reporting permeability as a function of porosity in fine-grained sediments. This standardization is particularly important for transferring results between locations with different smectite contents. The results presented in this study can be further refined through additional measurements of smectite content, and including sample-specific smectite correction such as for Costa Rica samples.

5.2. Grain size

Based on grain size classification, the observed differences in the siliciclastic permeability–porosity relationship appear to be correlated to the amount of clay- and silt-sized particles present in the sample. In the comparison to Bryant's (2002) permeability–porosity relationships,

Table 2
Permeability–porosity relationships based on grain size analyses using uncorrected and corrected porosities. Bryant's (2002) hydraulic conductivities were converted to permeability using a viscosity of 0.000966 Pa s and density of 1023 kg/m^3 at a temperature of 25 °C and a salinity of 35 kg/m^3.

Group	Description	Permeability–porosity relationship (uncorrected)	Permeability–porosity relationship (corrected)	Permeability–porosity relationship for Gulf of Mexico (Bryant 2002)
1	> 80% clay	$\log(k) = -24.3 + 11.3n$ ($R^2 = 0.53$)	$\log(k) = -24.6 + 13.3n$ ($R^2 = 0.46$)	$\log(k) = -20.9 + 6.5n$
2	60–80% clay	$\log(k) = -19.6 + 3.9n$ ($R^2 = 0.64$)	$\log(k) = -19.2 + 4.2n$ ($R^2 = 0.71$)	$\log(k) = -20.5 + 6.2n$
3	Silty-clays with <60% clay and <5% sand	$\log(k) = -19.4 + 4.4n$ ($R^2 = 0.40$)	$\log(k) = -18.4 + 3.1$ ($R^2 = 0.48$)	$\log(k) = -20.6 + 6.8n$

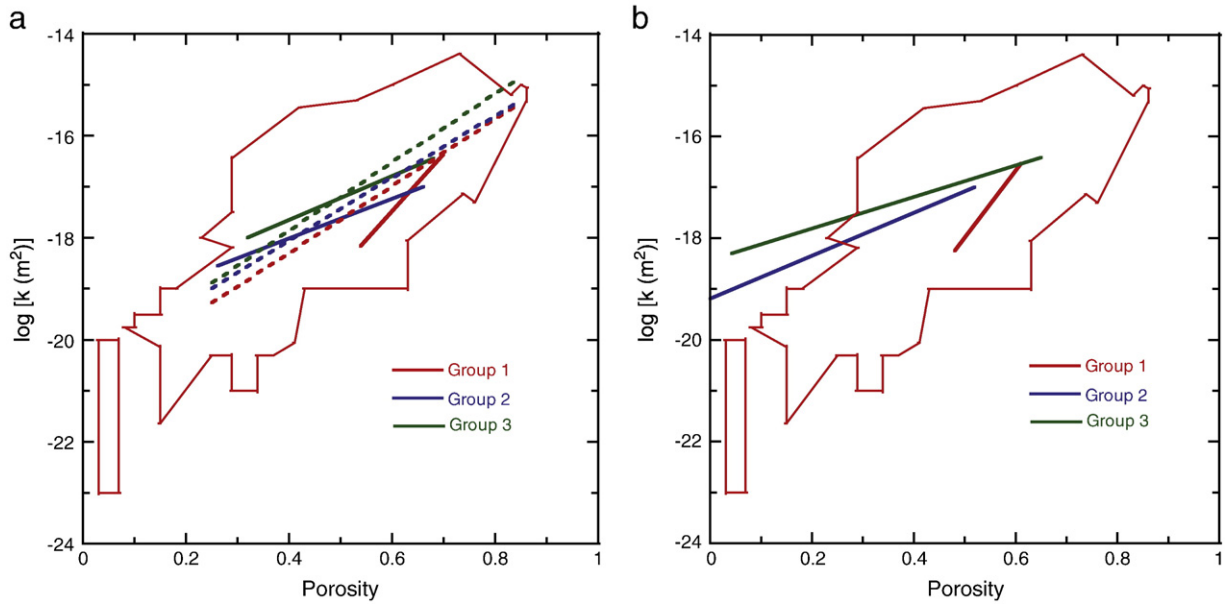

Fig. 3. a) Permeabilities classified based on grain size distribution using uncorrected porosity. Solid lines represent permeability–porosity relationship predicted for samples used in this study. Dashed line represents permeability–porosity relationships of Bryant (2002). b) Permeabilities classified based on grain size distribution using corrected porosity.

the largest discrepancy appeared in Group 1 (>80% clay-size material) and is likely related to the narrow range of porosities (0.50–0.70) in the dataset for this group. The predicted permeability–porosity relationships for Groups 2 (60%–80% clay-size material) and 3 (<60% clay-size material and >5% sand) are much closer to the relationships of Bryant (2002). Despite the fact that our samples represented different locations, the general permeability–porosity relationship exhibits a trend comparable to samples taken from a single location (e.g., Bryant (2002) samples from Gulf of Mexico) suggesting that grain size classification can be applicable across wide range of marine sediments. Ideally, plotting permeability as a function of clay-size material for constant porosity would further yield insight in terms of grain-size effect; however, data in this study were insufficient to allow analyses of this type. With respect to the lithological classification discussed below, using a quantitative approach such as grain size can provide a better global approximation for permeability–porosity relationships for siliciclastic sediments.

5.3. Lithologic grouping

5.3.1. Siliciclastic sediments

The combined siliciclastic permeability data from northern Barbados, Costa Rica, and Nankai subduction zones fall in the same general region of the permeability–porosity plot and represent a global approximation for the relation between permeability and porosity. Separating samples by their secondary lithological component and then

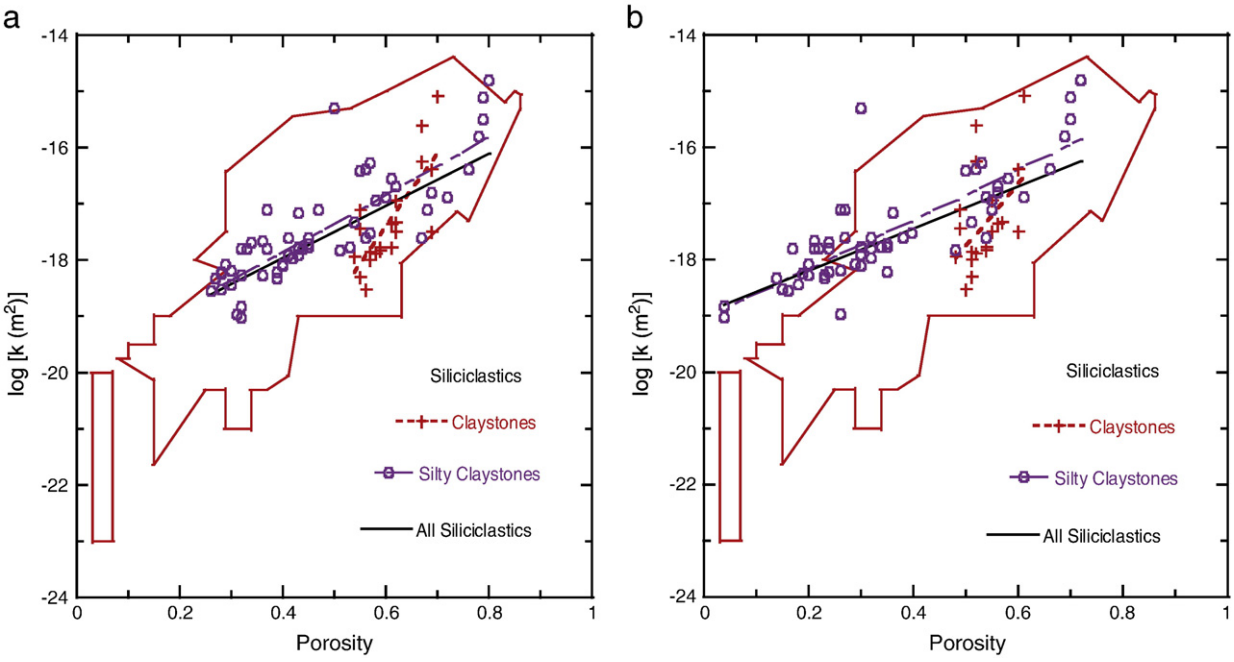

Fig. 4. Permeabilities and predicted log-linear permeability–porosity relationships for siliciclastic sediments using (a) uncorrected and (b) corrected (b) porosity.

Table 3
Log linear permeability–porosity relationships predicted for varying lithologies at Barbados, Costa Rica, Nankai and Peru. *Clay-rich diatom oozes include the following samples 201-1230A-4 H, 9 H, 31X, 35X and 205-1254A-16R-4, 1255A-3R-CC, 1255A-4R-CC. #Costa Rica include only one nannofossil ooze sample.

Lithologies and location	Permeability–porosity relationship (uncorrected porosity)	Permeability–porosity relationship (corrected porosity)
Siliciclastics		
Barbados claystones	$\log(k) = -25.3 + 13.2n$ ($R^2 = 0.60$)	$\log(k) = -23.3 + 11.2n$ ($R^2 = 0.23$)
Costa Rica silty claystones	$\log(k) = -20.6 + 6.1n$ ($R^2 = 0.63$)	$\log(k) = -18.8 + 4.3n$ ($R^2 = 0.63$)
Nankai silty claystones	$\log(k) = -19.8 + 5.2n$ ($R^2 = 0.72$)	$\log(k) = -19.1 + 4.1n$ ($R^2 = 0.77$)
Silty claystones (Costa Rica and Nankai)	$\log(k) = -19.9 + 5.1n$ ($R^2 = 0.69$)	$\log(k) = -19.1 + 4.5n$ ($R^2 = 0.68$)
All siliciclastics	$\log(k) = -19.8 + 4.6n$ ($R^2 = 0.55$)	$\log(k) = -19.0 + 3.9n$ ($R^2 = 0.50$)
Diatom oozes		
Costa Rica diatom oozes	$\log(k) = -20.4 + 4.9n$ ($R^2 = 0.82$)	$\log(k) = -19.0 + 3.5n$ ($R^2 = 0.73$)
Peru diatom oozes	$\log(k) = -17.3 + 1.0n$ ($R^2 = 0.19$)	$\log(k) = -17.2 + 0.9n$ ($R^2 = 0.24$)
All diatom oozeS	$\log(k) = -19.9 + 4.9n$ ($R^2 = 0.49$)	$\log(k) = -18.8 + 3.6n$ ($R^2 = 0.65$)
*Clay-rich diatom oozes (Peru and Costa Rica)		$\log(k) = -19.1 + 3.9n$ ($R^2 = 0.88$)
Nannofossil oozes and chalk		
Peru nannofossil oozes	$\log(k) = -15.2 + 0.4n$ ($R^2 = 0.02$)	
#All nannofossil oozes (Peru and Costa Rica)	$\log(k) = -14.5 - 1.3n$ ($R^2 = 0.07$)	
Peru nannofossil chalk	$\log(k) = -28.9 + 20.7n$ ($R^2 = 0.77$)	
Costa Rica nannofossil chalk	$\log(k) = -18.0 + 4.5n$ ($R^2 = 0.36$)	
All chalks	$\log(k) = -20.5 + 7.7n$ ($R^2 = 0.21$)	

by location predicted better constrained permeability–porosity relationships for each location. In the case of Barbados claystones, the permeability–porosity relationship showed scatter even within an individual location. These sediments from the Barbados décollement zone are radiolarian rich (Shipboard Scientific Party, 1995b). Radiolarian-rich sediments are resistant to consolidation during early burial (Hamilton, 1976), thus maintaining higher porosity due to intraskeletal pore spaces. Compared to other siliciclastics, Barbados claystones show a slower reduction in porosity with depth during shallow (<1 km) burial. When radiolarian-rich décollement samples were removed from the data set, the correlation between permeability and porosity improved from 17% to 72%. However, due to the statistically small sample size, this observation is inconclusive.

For silty claystones, samples from Costa Rica and Nankai yielded similar permeability–porosity relationships. This is somewhat surprising considering the very different thermal conditions (Costa Rica 9.6–7.2 °C/km and Nankai 60 –183 °C/km) at the two locations. In addition, Costa Rica and Nankai sediments contain varying amounts of biogenic silica, and dissolved silica was detected in pore waters, indicating dissolution (Shipboard Scientific Party, 1997b, c, 2001b, c, d, 2003e, f). Based on available smear slide data Nankai sediments may contain >1–5% diatoms while at Costa Rica diatom content varies from 0 to 20% (Shipboard Scientific Party, 1997a, b, 2001a, b, c, 2003c, e). As burial temperature increases, diatoms composed of biogenic opal-A dissolve. The dissolution of opal-A triggers precipitation of opal-CT as a coating on the sediment grains (Iijima and Tada, 1981). At Nankai, opal-CT coating on grain contacts was observed on samples from Sites 1173 and 1177 (Spinelli et al., 2007). Studies have shown that even a small amount of the opal-CT cement can increase the strength of the grains dramatically, thus inhibiting consolidation (Clough et al., 1981; Karig, 1993) with little or no noticeable change in porosity (e.g. Hamilton, 1976). Although this may help maintain porosity, it can decrease permeability as the cement clogs the pore throats thus affecting the permeability–porosity relationship as burial temperature increases. The similarity between Costa Rica and Nankai results suggests that, at least in these locations, the biogenic silica does not greatly affect results. Examining the amount of biogenic silica in silty clays from these two locations could further provide insight to the state of diagenesis of biogenic silica and its relation to the permeability–porosity relationship.

5.3.2. Diatom oozes

Porosity in diatom oozes in large part reflects the intraskeletal porosity of the diatoms (Bryant and Rack, 1990), which does not affect the permeability of the sediment. If opal-CT is precipitated, then the intraskeletal pore structure will be supported with little or no change in permeability. The combination of opal-CT cementation with the interweaving of the diatom tests further provides a rigid structure (Bryant et al., 1981). Despite this effect, the overall relationship predicted for the diatom oozes is comparable to that predicted for siliciclastic sediments. Generally, the diatom oozes with more abundant clay-size particles behave similarly to siliciclastics. For example, Costa Rica diatom oozes with >50% clay-sized particles show a good correlation between permeability and porosity while Peru diatom oozes with <50% clay-sized particles (with the exception of one sample from Core 201-1230A-35X) did not show a strong correlation between permeability and porosity. Instead, Peru samples contained >50% silt-size particles likely controlled by the size of diatoms. None of the diatom ooze samples used in this study have clay mineralogy data to assess whether the clay particle size actually represents clay minerals. Overall, the permeability data for diatom oozes presented here are comparable to the permeability values for siliceous-rich sediments given by Spinelli et al. (2004). Their general relationships for siliceous-rich sediments are similar to the relation of our siliciclastic sediments at ≥0.5 porosity.

5.3.3. Nannofossil oozes and chalks

For nannofossil oozes, mechanical compaction is the most prevalent factor that controls porosity at shallow depths. However at greater depths with the changes in temperature, pressure, and salinity, chemical compaction becomes more prevalent. For nannofossil oozes the most significant result compared to siliciclastics is the approximately 30-times higher permeability for a given porosity. The poor correlation between permeability and porosity suggests that early porosity reduction can occur without significant reduction in pore channels responsible for fluid flow. Porosity reduction in nannofossil ooze begins through mechanical compaction soon after it is deposited (Mallon and Swarbrick, 2002). During the first 50 m of burial, nannofossil ooze porosity can decrease by as much as 10% owing to mechanical compaction (Matter et al., 1975). Chemical compaction becomes more important around 200 m of burial depth, where precipitation of dissolved calcite decreases porosity to values as low as 0.25 (Mallon and Swarbrick, 2002). The nannofossil oozes in this study were predominantly located above chemical compaction depths, and the nannofossil chalks (300–600 mbsf) were within the dominant chemical compaction zone.

Although the Costa Rica and Peru nannofossil oozes did not improve correlation between permeability and porosity even after

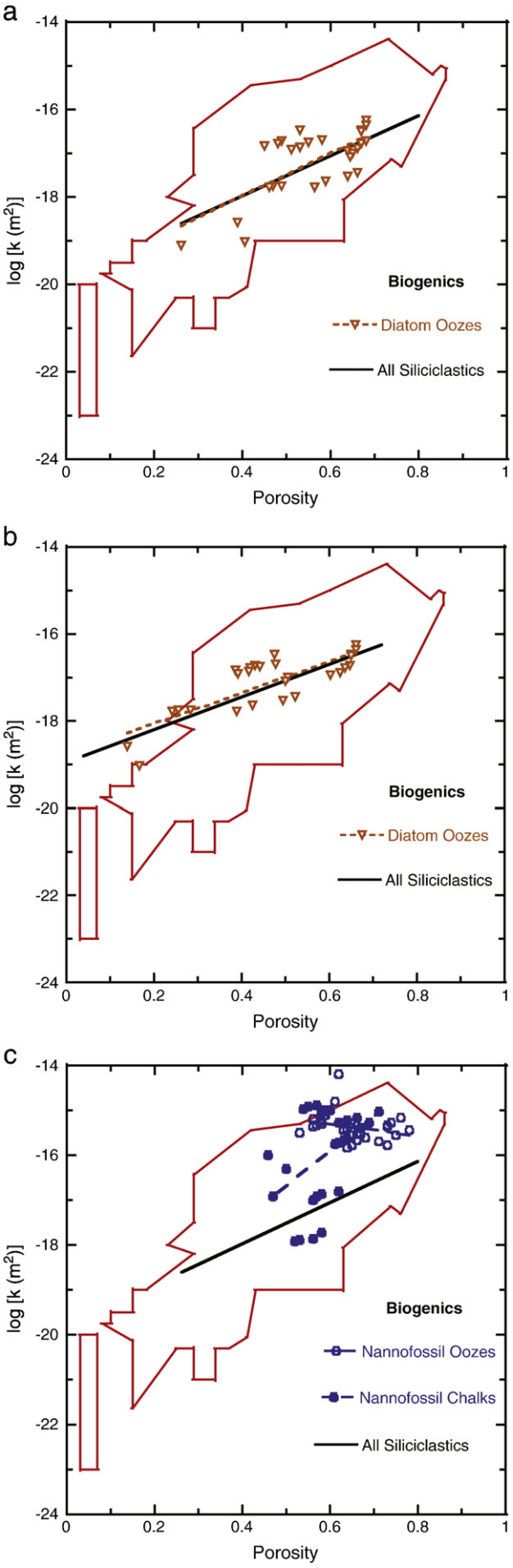

separating by location, the rapid change in porosity with burial depth seems similar to that predicted by Mallon and Swarbrick (2002) for carbonate oozes and chalks. Based on this observation, it is apparent that mechanical compaction is the primary process of porosity reduction for Peru nannofossil oozes. Although this may be also true for Costa Rica, the small sample size cannot confirm this conclusion without further investigation. Similar to the nannofossil oozes, the combined Costa Rica and Peru chalks show poor correlation between permeability and porosity. However, when separated by location the correlation improves signaling the differences in mechanical and/or chemical processes at the two locations. It is worth noting that nannofossil oozes and chalks from Costa Rica and Peru contain various amounts of diatoms (Table 1) and depending on the amount of diatoms present; the porosity may also be affected by the intraskeletal pore spaces and diagenesis of biogenic silica.

The data presented here are too limited for a full evaluation of chemical compaction. Overall, the upper permeability values of nannofossil chalk overlap nannofossil ooze permeabilities, suggesting nannofossil oozes represent the early mechanical compaction of nannofossil chalk. Interestingly, the lower values of the nannofossil chalks overlap siliciclastic permeabilities for porosities <0.6, suggesting similar consolidation patterns at depth. Similarly, Mallon et al. (2005) reported comparable permeability values of non reservoir chalks and shales over porosity range of 0.15–0.2.

5.4. Major findings and remaining questions

Results provide insight on variable controls on permeability–porosity relationships in subduction zone sediments. Based on the findings of this study, it is apparent that grain size, particularly the amount of clay-size material, is the major controlling factor in permeability–porosity relationships of siliciclastics and diatom oozes. In-situ temperatures of the Nankai sediments from offshore Muroto are sufficient for smectite to illite dehydration, and possible growth of clay minerals has been inferred to occur at grain boundaries (Morgan and Ask, 2004). In contrast, Costa Rica sediments have a very low thermal gradient, and thus have experienced little diagenesis. Despite great differences of in-situ temperatures, pressures, and resulting diagenetic states, the siliciclastic sediments show consistent permeability–porosity relationships.

In diatom oozes, the rigid framework reduces mechanical compaction. However, with increasing temperatures, the transformation of diatom oozes into authigenic aluminosilicate minerals (Cole, 1985; Banfield et al., 1991; Michalopoulos et al., 2000) may cause significant chemical compaction. This conversion process has also been linked to the transformation of smectite–illite phase to illite rich phase during burial diagenesis (Michalopoulos et al., 2000). This series of diagenetic processes may cause diatom oozes to behave more like siliciclastics with increasing diagenesis. Future work focused on diagenetic processes of biogenic silica will shed insight to various controls and applicability of permeability–porosity relationships for diatom oozes.

Sediments containing high clay contents with few impurities such as carbonates exhibit little diagenetic change with increasing depth (Bryant et al., 1981). As the carbonate content in siliciclastics increases, the overall reduction in porosity is less because the sediment structure can support greater overburden pressure compared to carbonate free siliciclastics (Bryant et al., 1981). As observed within the siliciclastic subgroups presented in this study, even minor lithological changes can change the permeability–porosity relationship as the degree of

Fig. 5. Permeabilities and predicted log-linear permeability–porosity relationships for biogenic sediments. a) diatom oozes using uncorrected porosity and b) diatom oozes using corrected porosity. c) nannofossil oozes and nannofossil chalks using uncorrected porosity.

compaction varies with the amount of clay minerals present in the sediment.

In contrast to siliciclastic sediments, permeability–porosity relationships for nannofossil ooze and chalk do not show a good correlation. In general carbonates do not consolidate as much as non carbonates (Bryant et al., 1981). This difference may relate to the variable response to mechanical and chemical compaction caused by minor lithological variations (impurities), smectite content, intraskeletal pore structures and strength of individual particles. For example, porosities of clean chalk are mainly controlled by diagenetic processes during chemical compaction while for argillaceous chalk both mechanical and chemical compaction play an important role (Mallon et al., 2005).

The data suggest greater variation in the behavior of high-porosity sediments, likely due to variable amounts of biogenic components. Thus, detailed site-specific permeability results may be necessary for studies of fluid flow during early burial. In contrast, the various sediment types show more similar permeability–porosity behavior at lower porosities. Further data are needed from a wide range of settings, but it is possible that, reasonable permeability–porosity relationships may be inferred from grain-size data for studies that are not affected by shallow processes.

5.5. Standardized test protocols and future work

Apart from a large range of effects from mechanical and chemical compaction, human and machinery errors can also contribute to some of the variations observed in measured permeability, porosity and smectite data. Although we do not have sufficient information to quantify these errors, the following section briefly summarizes some of the main issues. For example, soft sediments recovered using the hydraulic piston core (also known as advanced piston coring or APC) system are generally undisturbed compared to more lithified samples recovered using the extended core barrel (XCB) or rotary core barrel (RCB) coring system. Coring disturbances and drying out can disrupt the sedimentary fabric, affecting the measured permeabilities. During permeability testing, minute leaks in the apparatus, deterioration, and disturbance of the specimen can also affect measured permeability, particularly in fine-grained sediments (e.g. Neuzil, 1994).

When estimating smectite content, a common error identified is related to the process of disaggregating highly compacted sediments (personal communication, M. Underwood, 2007). As compaction progresses, disaggregation of sediments becomes challenging, especially when clay minerals exist within the fine silt fraction. Because particle shapes deviate significantly from perfect spheres, inaccuracies are introduced when partitioning clay minerals in different proportions within different ranges of grain size. Overall, the inaccuracies introduced by the methods used to quantify smectite content have to be evaluated and possibly quantified to improve accuracy.

Assembling data for this study made it apparent that some of the critical parameters such as temperature, type of permeant, void ratio, grain size, carbonate, and smectite content were not clearly documented or were never measured. Availability of such fundamental data is indispensable in quantifying meaningful relationships between permeability and porosity. Without doubt, future studies should make all effort to collect/measure critical physical properties data routinely to contribute to the much-needed marine sediment database.

Due to the limited number of samples from the prism environment, this study could not assess the role of horizontal shortening on the permeability–porosity relationship. The limited data suggest some differences (Gamage, 2005) but results are inconclusive. With the availability of new technology, future sampling should focus on retrieving samples from the full range of structural domains (e.g., prism, décollement, underthrust) at varying depths and high resolution.

6. Conclusions

We examined permeability–porosity relationships for sediments from four different subduction zones based on sediment type, grain size distribution, and general compaction history. Although data used in this study mainly represent sediments from subduction settings, the overall findings may be more broadly applicable to a wide range of marine sediments.

Overall, a greater effect of porosity on permeability was observed for siliciclastic sediments, diatom oozes, and nannofossil chalks than for nannofossil oozes. Correcting porosity values to exclude smectite interlayer water improved permeability–porosity relationships. For siliciclastic sediments using a quantitative approach such as grain size can provide a better global approximation for permeability–porosity relationships. The overall relationship predicted for diatom oozes is very similar to that predicted for siliciclastic sediments and is closely related to the amount of clay size particles present in the sediment. Nannofossil ooze permeabilities were 1.5 orders of magnitude greater than siliciclastic sediments for a given porosity. The nannofossil oozes did not demonstrate a strong correlation between porosity and permeability suggesting that early porosity reduction can occur without significant reduction in pore channels responsible for fluid flow.

Categorizing samples by their lithological components and then by location predicted more constrained permeability–porosity relationships for each location. However, descriptive lithologic classifications are more challenging when used across many different data sets that were originally based on different classification schemes. It was evident that secondary constituents can decrease permeability–porosity correlations and, thus, careful consideration of lithology is recommended. To further investigate and delineate the controls on permeability and porosity, it is essential to consider effects of both mechanical and chemical compaction on well-defined samples. Additional information, such as site-specific smectite contents as well as reducing errors associated with methodology will help further improve porosity estimates. Other factors such as core disturbances and experimental errors should be minimized as these contribute to large variations in measured permeabilities.

Supplementary materials related to this article can be found online at doi:10.1016/j.margeo.2010.10.010.

Acknowledgements

This research used samples and data provided by the Ocean Drilling Program (ODP). ODP was sponsored by the U.S. National Science Foundation (NSF) and participating countries under the management of Joint Oceanographic Institutions (JOI), Inc. We especially want to thank Mike Underwood and Dawn Cardace for use of their data. This manuscript has benefited greatly from valuable and thorough reviews by the Editor David Piper, Chris Neuzil, Steve Ingebritsen, Angelo Camerlenghi, and two anonymous reviewers. Funding for this research was provided by JOI/United States Science Support Program (USSSP) postcruise grants to E. Screaton and B. Bekins and by the NSF through grant OCE-0751497 to E. Screaton.

References

Aiello, I.W., Kellett, K., 2006. Sedimentology of open-ocean biogenic sediments from ODP Leg 201, eastern equatorial Pacific (Sites 1225 and 1226). In: Jørgensen, B.B., D'Hondt, S.L., Miller, D.J. (Eds.), Proceedings of the Ocean Drilling Program, Scientific Results, 201. Ocean Drilling Program, College Station, TX, pp. 1–25. doi:10.2973/odp.proc.sr.201.112.2006.

Alpin, A.C., Fleet, A.J., Macquaker, J.H.S., 1999. Muds and mudstones: physical and fluid flow properties. The Geological Society of London, Special Publications, 158, pp. 1–8.

Banfield, J.F., Jones, B., Veblen, D., 1991. An AEM-TEM study of weathering and diagenesis, Abert Lake, Oregon: II. Diagenetic modification of the sedimentary assemblage. Geochimica et Cosmochimica Acta 55, 2795–2810.

Bekins, B.A., McCaffrey, A.M., Dreiss, S.J., 1995. Episodic and constant flow models for the origin of low-chloride waters in a modern accretionary complex. Water Resources Research 31, 3205–3215.

Bennett, R.H., Fischer, K.M., Lavoie, D.L., Bryant, W.R., Rezak, R., 1989. Porometry and fabric of marine clay and carbonate sediments: determinants of permeability. Marine Geology 89, 127–152.
Boggs, S., 2001. Principles of sedimentology and stratigraphy. Prentice-Hall, Inc, New Jersey, pp. 378–416.
Bolton, A., Maltman, A., 1998. Fluid-flow pathways in actively deforming sediments: the role of pore fluid pressure and volume change. Marine and Petroleum Geology 15, 281–297.
Bolton, A., Maltman, A.J., Fisher, Q., 2000. Anisotroptic permeability and bimodal pore-size distributions of fine-grained marine sediments. Marine and Petroleum Geology 17, 657–672.
Brown, K.M., Moore, C., 1993. Anisotropic permeability and tortuosity in deformed wet sediments. In: Arch, J., Maltman, A. (Eds.), Journal of Geophysical Research, 98, pp. 17859–17864.
Brown, K.M., Ransom, B., 1996. Porosity corrections for smectite-rich sediments: impact on studies of compaction, fluid generation, and tectonic history. Geology 24, 843–846.
Brown, K.M., Saffer, D.M., Bekins, B.A., 2001. Smectite diagenesis, pore-water freshening, and fluid flow at the toe of the Nankai wedge. Earth and Planetary Science Letters 194, 97–109.
Bruckmann, W., Moran, K., Mackillop, A., 1997. Permeability and consolidation characteristics from Hole 949B, northern Barbados Ridge. Proceedings of the Ocean Drilling Program, Scientific Results 156, 109–114.
Bryant, W.R., 2002. Permeability of clays, silty-clays and clayey-silts. Gulf Coast Association of Geological Societies Transactions 52, 1069–1077.
Bryant, W.R., Bennett, R., Katherman, C., 1981. Shear strength, consolidation, porosity, and permeability of oceanic sediments. In: Emiliani, C. (Ed.), The Sea. Wiley, New York, pp. 1555–1616.
Bryant, W.R., Hottman, W., Trabant, P., 1975. Permeability of unconsolidated and consolidated marine sediments, Gulf of Mexico. Marine Geotechnology 1, 1–14.
Bryant, W.R., Rack, F.R., 1990. Consolidation characteristics of Weddell Sea sediments: results of ODP Leg 113. In: Barker, P.F., Kennett, J.P., et al. (Eds.), Proceedings of the Ocean Drilling Program, Scientific Results, 113. Ocean Drilling Program, College Station, TX, pp. 211–223. doi:10.2973/odp.proc.sr.113.173.1990. [Accessed 2010-07-27].
Cardace, D., 2006. Dissertation: Geochemistry, Mineralogy, Geobiology of Subducting Sediments at the Costa Rican Convergent Margin, ProQuest Information and Learning Company, MI.
Clennell, M.B., Dewhurst, D.N., Brown, K.M., Westbrook, G.K., 1999. Permeability anisotropy of consolidated clays. In: Aplin, A.C., Fleet, A.J., Macquaker, J.H.S. (Eds.), Mu and Mudstones: Physical and Fluid Flow Properties. Geological Society, Special Publications, 158. London, pp. 79–96.
Clough, G.W., Sitar, N., Bachus, R.C., Rad, N.S., 1981. Cemented sands under static loading. Journal of the Geotechnical Engineering Division 107, 799–817.
Cole, T.G., 1985. Composition, oxygen isotope geochemistry, and origin of smectite in the metalliferous sediments of the Bauer Deep, southeast Pacific. Geochimica et Cosmochimica Acta 49, 221–235.
Colten-Bradley, V.A., 1987. Role of pressure in smectite dehydration-effects on geopressures and smectite-to-illite transformation. The American Association of Petroleum Geologists Bulletin 71, 1414–1427.
D'Hondt, S.L., Jørgensen, B.B., Miller, D.J., et al., 2003. Proceedings of the Ocean Drilling Program, Initial Reports, 201. Ocean Drilling Program, College Station, TX. doi:10.2973/odp.proc.ir.201.2003.
DeMets, C., Gordon, R.G., Argus, D.F., Stein, S., 1990. Current plate motions. Geophysical Journal International 101, 425–478.
Dewhurst, D.N., Yang, Y., Alpin, A., 1999. Permeability and flow in natural mudstones. In: Alpin, A.C., Fleet, A.J., Macquaker, J.H.S. (Eds.), Muds and Mudstones: Physical and Fluid Flow Properties, 158. Geological Society, Special Publications, London, pp. 23–43.
Fetter, C.W., 1994. Applied Hydrogeology, third ed. Prentice Hall, New Jersey.
Fisher, A.T., Hounslow, M.W., 1990. Transient fluid flow through the toe of the Barbados accretionary complex: constraints from Ocean Drilling Program Leg 110 heat flow studies and simple models. Journal of Geophysical Research 95, 8845–8858.
Gamage, K., 2005. Dissertation: permeabilities of subduction zone sediments and their effect on pore pressure generation. University of Florida, Gainesville, FL.
Gamage, K., Bekins, B., Screaton, E., 2005. Data report: Permeabilities of eastern equatorial Pacific and Peru margin sediments., in: Jørgensen, B.B., D'Hondt, S.L., Miller, D.J., et al. (Ed.), Proceedings of the Ocean Drilling Program, Scientific Results, 201 [Online]. Available from World Wide Web: <http://www-odp.tamu.edu/publications/201_SR/103/103.htm>. [Accessed 2005-07-11].
Gamage, K., Screaton, E., 2003. Data report: permeabilities of Nankai accretionary prism sediments. In: Mikada, H., Moore, G.F., Taira, A., Becker, K., Moore, J.C., Klaus, A. (Eds.), Proceedings of the Ocean Drilling Program, Scientific Results 190/196, pp. 1–22. [Online]. Available from World Wide Web<http://www-odp.tamu.edu/publications/190196SR/VOLUME/CHAPTERS/213.PDF>. [Accessed 2004-06-10].
Gamage, K., Screaton, E., 2006. Characterization of excess pore pressures at the toe of the Nankai accretionary complex, Ocean Drilling Program sites 1173, 1174, and 808: results of one-dimensional modeling. Journal of Geophysical Research 111, B04103. doi:10.1029/2004JB003572.
Hamilton, E.L., 1976. Variations of Density and Porosity with depth in Deep-Sea sediments. Journal of Sedimentary Petrology 46, 280–300.
Hampel, A., 2002. The migration history of the Nazca Ridge along the Peruvian active margin: a re-evaluation. Earth and Planetary Science Letters 203, 665–679.
Hubbert, M.K., Rubey, W.W., 1959. Role of fluid pressure in mechanics of overthrust faulting. Geological Society of America Bulletin 70, 115–166.
Iijima, A., Tada, R., 1981. Silica diagenesis of neogene diatomaceous and volcaniclastic sediments in northern Japan. Sedimentology 28, 185–200.
Karig, D., 1993. Reconsolidation tests and sonic velocity measurements of clay-rich sediments from the Nankai Trough. In: Hill, I.A., Taira, A., et al. (Eds.), Proceedings of the Ocean Drilling Program, Scientific Results, 131, College Station, TX, pp. 247–260.
Koltermann, C., Gorelick, M., 1995. Fractional packing model for hydraulic conductivity derived from sediment mixtures. Water Resources Research 31, 3283–3297.
Langseth, M.G., Silver, E.A., 1996. The Nicoya convergent margin-a region of exceptionally low heat flow. Geophysical Research Letters 23, 891–894.
Mallon, A.J., Swarbrick, R.E., 2002. A compaction trend for non-reservoir North Sea Chalk. Marine and Petroleum Geology 19, 527–539.
Mallon, A.J., Swarbrick, R.E., Katsube, T.J., 2005. Permeability of fine-grained rocks: new evidence from chalks. Geology 33, 21–24.
Matmon, D., Bekins, B.A., 2006. Hydromechanics of a high taper angle, low permeability prism: a case study from Peru. Journal of Geophysical Research 111.
Matter, A., Douglas, R.G., Perch-Nielsen, K., 1975. Fossil preservation, geochemistry and diagenesis of pelagic carbonates from Shatsky rise, northwest Pacific. Initial Reports Deep Sea Drilling Project 32, 891–922. doi:10.2973/dsdp.proc.32.137.1975.
Mazzullo, J.M., Meyer, A., Kidd, R.B., 1988. New sediment classification scheme for the Ocean Drilling Program. In: Mazzullo, J., Graham, A.G. (Eds.), Handbook for Shipboard Sedimentologists. ODP Technical Notes, pp. 45–67.
Mcconnachie, I., 1974. Fabric changes in consolidated kaolin. Geotechnique 24 (207), 222.
McKiernan, A.W., Saffer, D.M., 2006. Data report: Permeability and consolidation properties of subducting sediments off Costa Rica, ODP Leg 205, in: Morris, J.M., Villinger, H.W., Klaus, A. (Ed.). Proceedings of the Ocean Drilling Program, Scientific Results 205, 1-24 [Online]. Available from World Wide Web: <http://www-odp.tamu.edu/publications/205_SR/VOLUME/CHAPTERS/203.PDF> [Accessed 2005-05-30].
Meyer, A., Fisher, A., 1997. Data report: grain-size analysis of sediments from the northern Barbados accretionary prism. In: Shipley, T.H., Ogawa, Y., Blum, P., Bahr, J.M. (Eds.), Proceedings of the Ocean Drilling Program, Scientific Results, 156. Ocean Drilling Program, College Station, TX, pp. 337–341. doi:10.2973/odp.proc.sr.156.005.1997.
Michalopoulos, P., Aller, R.C., Reeder, R.J., 2000. Conversion of diatoms to clays during early diagenesis in tropical, continental shelf muds. Geology 28, 1095–1098.
Morgan, J.K., Ask, M.V.S., 2004. Consolidation state and strength of underthrust sediments and evolution of the décollement at the Nankai accretionary margin: results of uniaxial reconsolidation experiments. Journal of Geophysical Research 109. doi:10.1029/2002JB002335.
Neuzil, C.E., 1994. How permeable are clays and shales. Water Resources Research 30, 145–150.
Saffer, D.M., Bekins, B.A., 1998. Episodic fluid flow in the Nankai accretionary complex: timescale, geochemistry, flow rates, and fluid budget. Journal of Geophysical Research-Solid Earth 103, 30351–30370.
Saffer, D.M., McKiernan, A.W., 2005. Permeability of underthrust sediments at the Costa Rican margin: scale dependence and implications for dewatering. Geophysical Research Letters 32, L02302. doi:10.1029/2004GL021388.
Saffer, D.M., Silver, E.A., Fisher, A.T., Tobin, H., Moran, K., 2000. Inferred pore pressures at the Costa Rica subduction zone: implications for dewatering processes. Earth and Planetary Science Letters 177, 193–207.
Screaton, E.J., Hays, T., Gamage, K., Martin, J., 2006. Data report: Permeabilities of Costa Rica subduction zone sediments, in: Morris, J.M., Villinger, H.W., Klaus, A. (Ed.), Proceedings of the Ocean Drilling Program, Scientific Results, 205, 1-13 [Online]. Available from World Wide Web: <http://www-odp.tamu.edu/publications/205_SR/VOLUME/CHAPTERS/203.PDF>. [Accessed 2005-05-30].
Seno, T., Stein, S., Gripp, A.E., 1993. A model for the motion of the Philippine Sea Plate consistent with NUVEL-1 and geological data. Journal of Geophysical Research 98, 17,941-917, 948.
Shipboard Scientific Party, 1995a. Site 948, in: T. H., O., Y., Blum, P., et al. (Ed.), In Shipley, T.H., Ogawa, Y., Blum, P., et al., Proceedings of the Ocean Drilling Program, Initial Reports, 156: College Station, TX (Ocean Drilling Program), 87-192. doi:10.2973/odp.proc.ir.156.106.1995.
Shipboard Scientific Party, 1995b. Site 949. In: Shipley, T.H., Ogawa, Y., Blum, P., et al. (Eds.), Proceedings of the Ocean Drilling Program, Initial Reports, 156. Ocean Drilling Program, College Station, TX, pp. 193–257. doi:10.2973/odp.proc.ir.156.107.1995.
Shipboard Scientific Party, 1997a. Introduction. In: Kimura, G., Silver, E., Blum, P., et al. (Eds.), Proceedings of the Ocean Drilling Program, Initial Reports, 170. Ocean Drilling Program, College Station, TX, pp. 7–17. doi:10.2973/odp.proc.ir.170.101.1997.
Shipboard Scientific Party, 1997b. Site 1039. In: Kimura, G., Silver, E., Blum, P., et al. (Eds.), Proceedings of the Ocean Drilling Program, Initial Reports, 170. Ocean Drilling Program, College Station, TX, pp. 45–93. doi:10.2973/odp.proc.ir.170.103.1997.
Shipboard Scientific Party, 1997c. Site 1040, in: Kimura, G., Silver, E., Blum, P., et al. (Ed.), In Kimura, G., Silver, E., Blum, P., et al., Proceedings of the Ocean Drilling Program, Initial Reports, 170: College Station, TX (Ocean Drilling Program), 95–152. doi:10.2973/odp.proc.ir.170.104.1997.
Shipboard Scientific Party, 2001a. Leg 190 summary. In: Moore, G.F., Taira, A., Klaus, A., et al. (Eds.), Proceedings of the Ocean Drilling Program, Initial Reports, 190. Ocean Drilling Program, College Station, TX, pp. 1–87. doi:10.2973/odp.proc.ir.190.101.2001.
Shipboard Scientific Party, 2001b. Site 1173. In: Moore, G.F., Taira, A., Klaus, A., et al. (Eds.), Proceedings of the Ocean Drilling Program, Initial Reports, 190. Ocean Drilling Program, College Station, TX, pp. 1–147. doi:10.2973/odp.proc.ir.190.104.2001.
Shipboard Scientific Party, 2001c. Site 1174. In: Moore, G.F., Taira, A., Klaus, A., et al. (Eds.), Proceedings of the Ocean Drilling Program, Initial Reports, 190. Ocean Drilling Program, College Station, TX, pp. 1–149. doi:10.2973/odp.proc.ir.190.105.2001.
Shipboard Scientific Party, 2001d. Site 1177. In: Moore, G.F., Taira, A., Klaus, A., et al. (Eds.), Proceedings of the Ocean Drilling Program, Initial Reports, 190. Ocean Drilling Program, College Station, TX, pp. 1–91. doi:10.2973/odp.proc.ir.190.108.2001.

Shipboard Scientific Party, 2003a. Site 1225. In: D'Hondt, S.L., Jørgensen, B.B., Miller, D.J., et al. (Eds.), Proceedings of the Ocean Drilling Program, Initial Reports, 201. Ocean Drilling Program, College Station, TX, pp. 1–86. doi:10.2973/odp.proc.ir.201.106.2003.

Shipboard Scientific Party, 2003b. Site 1226. In: D'Hondt, S.L., Jørgensen, B.B., Miller, D.J., et al. (Eds.), Proceedings of the Ocean Drilling Program, Initial Reports, 201. Ocean Drilling Program, College Station, TX, pp. 1–96. doi:10.2973/odp.proc.ir.201.107.2003.

Shipboard Scientific Party, 2003c. Site 1230. In: D'Hondt, S.L., Jørgensen, B.B., Miller, D.J., et al. (Eds.), Proceedings of the Ocean Drilling Program, Initial Reports, 201. Ocean Drilling Program, College Station, TX, pp. 1–107. doi:10.2973/odp.proc.ir.201.111.2003.

Shipboard Scientific Party, 2003d. Site 1231. In: D'Hondt, S.L., Jørgensen, B.B., Miller, D.J., et al. (Eds.), Proceedings of the Ocean Drilling Program, Initial Reports, 201. Ocean Drilling Program, College Station, TX, pp. 1–64. doi:10.2973/odp.proc.ir.201.112.2003.

Shipboard Scientific Party, 2003e. Site 1254. In: Morris, J.D., Villinger, H.W., Klaus, A., et al. (Eds.), Proceedings of the Ocean Drilling Program, Initial Reports, 205. Ocean Drilling Program, College Station, TX, pp. 1–113. doi:10.2973/odp.proc.ir.205.105.2003.

Shipboard Scientific Party, 2003 f. Site 1255. Shipboard Scientific Party, 2003. Site 1255. In Morris, J.D., Villinger, H.W., Klaus, A., et al., Proceedings of the Ocean Drilling Program, Initial Reports, 205: College Station, TX (Ocean Drilling Program), 1-55. doi:10.2973/odp.proc.ir.205.106.2003.

Silver, E., Kastner, M., Fisher, A., Morris, J., McIntosh, K., Saffer, D., 2000. Fluid flow paths in the Middle America Trench and Costa Rica margin. Geology 28, 679–682.

Skarbek, R.M., Saffer, D.M., 2009. Pore pressure development beneath the de´collement at the Nankai subduction zone: implications for plate boundary fault strength and sediment dewatering. Journal of Geophysical Research 114, B07401. doi:10.1029/2008JB006205.

Spinelli, G.A., et al., 2007. Diagenesis, sediment strength, and pore collapse in sediment approaching the Nankai through subduction zone. GSA Bulletin 119 (3/4), 377–390.

Spinelli, G.A., Giambalvo, E.R., Fisher, A.T., 2004. Sediment permeability, distribution, and influence on fluxes in oceanic basement. Hydrogeology of the Oceanic Lithosphere 151–188.

Spinelli, G.A., Underwood, M.B., 2004. Character of sediments entering the Costa Rica subduction zone: implications for partitioning of water along the plate interface. The Island Arc 13, 432–451.

Steurer, J.F., Underwood, M., 2003a. Data report: The relation between physical properties and grain-size variations in hemipelagic sediments from Nankai Trough, in: Mikada, H., Moore, G.F., Taira, A., Becker, K., Moore, J.C., Klaus, A. (Ed.), Proceedings of the Ocean Drilling Program, Scientific Results, 190/196, 1-25 [Online]. Available from World Wide Web<http://www-odp.tamu.edu/publications/190196SR/VOLUME/CHAPTERS/210.PDF>. [Accessed 2004-12-10].

Steurer, J.F., Underwood, M.B., 2003b. Clay mineralogy of mudstones from the Nankai Trough reference Sites 1173 and 1177 and frontal accretionary prism Site 1174, in: Mikada, H., Moore, G.F., Taira, A., Becker, K., Moore, J.C., and Klaus, A. (Ed.), Proceedings of the Ocean Drilling Program, Scientific Results, 190/196, 1-37 [Online]. Available from World Wide Web: <http://www-odp.tamu.edu/publications/190196SR/VOLUME/CHAPTERS/211.PDF>. [Accessed 2007-4-25].

Taylor, E., Leonard, J., 1990. Sediment consolidation and permeability at the Barbados forearc. In: Moore, J.C., Mascle, A., et al. (Eds.), Proceedings of the Ocean Drilling Program, Scientific Results, 110. Ocean Drilling Program, College Station, TX, pp. 289–308. doi:10.2973/odp.proc.sr.110.152.1990.

Tribble, J.S., 1990. Clay diagenesis in the Barbados Accretionary Complex: potential impact on hydrology and subduction dynamics. In: Moore, J.C., Mascle, A., et al. (Eds.), Proceedings of the Ocean Drilling Program, Scientific Results, 110. Ocean Drilling Program, College Station, TX, pp. 97–110. doi:10.2973/odp.proc.sr.110.131.1990.

Underwood, M.B., Deng, X., 1997. Clay mineralogy and clay geochemistry in the vicinity of the décollement zone, northern Barbados ridge. In: Shipley, T.H., Ogawa, Y., Blum, P., Bahr, J.M. (Eds.), *Proc.ODP, Sci. Results,* 156. [Online]. Available from World Wide Web:<http://www-odp.tamu.edu/publications/156_SR/01_CHP.PDF≥. [Cited 2006-03-01].

Zwart, G., Brückmann, W., Moran, K., MacKillop, A.K., Maltman, A.J., Bolton, A., Vrolijk, P., Miller, T., Gooch, M.J., Fisher, A.T., 1997. Evaluation of hydrogeologic properties of the Barbados accretionary prism: a synthesis of Leg 156 results. In: Shipley, T.H., Ogawa, Y., Blum, P., Bahr, J.M. (Eds.), Proceedings of the Ocean Drilling Program, Scientific Results, 156. Ocean Drilling Program, College Station, TX, pp. 303–310. doi:10.2973/odp.proc.sr.156.036.1997.